PolyPublie
Polytechnique Montréal

POLYTECHNIQUE MONTRÉAL
UNIVERSITÉ D'INGÉNIERIE

Titre: Title:	Impact of Vibratory Peening on The Surface Integrity of Cemented Steel E16NCD13
Auteur: Author:	Khouloud Chouchane
Date:	2021
Type:	Mémoire ou thèse / Dissertation or Thesis
Référence: Citation:	Chouchane, K. (2021). Impact of Vibratory Peening on The Surface Integrity of Cemented Steel E16NCD13 [Mémoire de maîtrise, Polytechnique Montréal]. PolyPublie. https://publications.polymtl.ca/9917/

Document en libre accès dans PolyPublie
Open Access document in PolyPublie

URL de PolyPublie: PolyPublie URL:	https://publications.polymtl.ca/9917/
Directeurs de recherche: Advisors:	Martin Lévesque, & Sylvain Turenne
Programme: Program:	Génie mécanique

Ce fichier a été téléchargé à partir de PolyPublie, le dépôt institutionnel de Polytechnique Montréal
This file has been downloaded from PolyPublie, the institutional repository of Polytechnique Montréal

https://publications.polymtl.ca

POLYTECHNIQUE MONTRÉAL
affiliée à l'Université de Montréal

Impact of Vibratory Peening on The Surface Integrity of Cemented Steel E16NCD13

KHOULOUD CHOUCHANE
Département de génie mécanique

Mémoire présenté en vue de l'obtention du diplôme de *Maîtrise ès sciences appliquées*
Génie mécanique

Décembre 2021

© Khouloud Chouchane, 2021.

POLYTECHNIQUE MONTRÉAL
affiliée à l'Université de Montréal

Ce mémoire intitulé :

Impact of Vibratory Peening on The Surface Integrity of Cemented Steel E16NCD13

présenté par **Khouloud CHOUCHANE**
en vue de l'obtention du diplôme de *Maîtrise ès sciences appliquées*
a été dûment accepté par le jury d'examen constitué de :

Étienne ROBERT, président
Martin LÉVESQUE, membre et directeur de recherche
Sylvain TURENNE, membre et codirecteur de recherche
Jérôme VÉTEL, membre

DEDICATION

To my lovely parents,
I am happy to see that you are now
reaping the fruits of your sacrifices.
As a token of my deep love and gratitude
for the support and care you have given me
with so much encouragement and sacrifice,

To my brothers and their little families,
you who admire me so much,
be sure that this work is the result
of your encouragement and your confidence in me.

To my grandparents,
in recognition of your encouragement
and moral support.

To my fiancé,
thank you for all your love and support.

To all those I love and that I did not mention.
. . .

ACKNOWLEDGEMENTS

I would like to express my sincere gratitude to prof. Martin Lévesque, my director, and to prof. Sylvain Turenne, my co-director, for the invaluable opportunity to pursue a master's degree under their supervisions. Their supports and the discussions we had fueled me throughout this work.

I am also very grateful to Dr. Hongyan Miao. She taught me how to conduct research, think and express myself. She helped me to gain knowledge in this field and also helped to improve my writing and speaking skills. I am grateful for her great contributions to this project.

Many thanks also to all industrial members of the project: Dr. Benoit Changeux and Dr. Jawad Badreddine from Safran Tech for guiding me and supervising me during this research work. Many thanks to the organization itself for its participation in the project.

I would also like to thank the technical team at CTA, Marie-Chrisitne Caya and Jeremy Elsek-Valois for their time and experience while conducting my experiments. I am also thankful for the help and support I received from Pr. Bernard Clément while planning the experiments.

I would like also to thank Safran Tech and Natural Sciences and Engineering Research Council of Canada (NSERC) for financing the project.

I would like to acknowledge the contribution of my coworker on this project, Maxime Paques. A special thanks goes to my best friend Abouthaina Saadallah for her help, support and encouragements that kept me motivated during all the project. Thanks also to all the LM2 laboratory for their support.

Finally, I would like to thank my family and my friends for being there for me throughout the good and bad times over the past years. I could not have done it without your support.

RÉSUMÉ

Le grenaillage vibratoire est un procédé alternatif qui vise à remplacer les procédés de grenaillage conventionnel et finition vibratoire. Il produit des contraintes résiduelles de compression comparables à celles obtenues par grenaillage coventionnel, mais avec un meilleur fini de surface, ce qui est censé améliorer la résistance à la fatigue de la pièce traitée. On pense également qu'elle améliore la productivité industrielle en combinant les étapes de grenaillage conventionnel et de finition vibratoire en un seul procédé. Bien qu'il existe des études sur ce procédé, aucun travail fondamental et physique présentant l'amélioration des propriétés générées n'a été présenté.

Cette étude fait partie d'un projet visant à démontrer les effets bénéfiques des technologies avancées de traitement de surface sur certains matériaux aérospatiaux qui était une collaboration entre Polytechnique Montréal, Safran Tech France et le Centre aérospatial et technologique de Longueuil (CTA). Ce travail a porté sur le calibration de la machine de grenaillage vibratoire et l'identification des limites de ses paramètres. Il comprend également l'étude de l'effet du grenaillage vibratoire sur les propriétés d'intégrité de surface de l'acier cémenté E16NCD13 en termes de rugosité de surface, de contraintes résiduelles de compression et de microdureté. Les modifications de l'intégrité de surface produites par le grenaillage vibratoire ont été comparées au grenaillage coventionnel à des intensités Almen similaires.

La revue de la littérature a montré que l'intensité Almen, le temps de traitement, l'amplitude, la fréquence, le poids des billes et la position de la pièce, etc. sont les paramètres clés du procédé de grenaillage vibratoire. La première partie de cette étude a présenté la relation entre les paramètres de la machine, tels que : le poids des billes, les masses excentriques, la fréquence, la pression, la hauteur des billes au-dessus de la pièce, la position de la pièce et le taux de lubrification avec l'amplitude de vibration de la machine et l'intensité Almen à l'aide de techniques de plans d'expériences. Les résultats ont montré que l'amplitude de vibration de la machine est principalement contrôlée par les masses excentriques sur les arbres rotatifs, la fréquence de rotation des arbres rotatifs, la hauteur des billes au-dessus de la pièce, et l'intensité Almen est principalement influencée par les les masses excentriques. Les résultats de plans d'expériences ont montré que la machine de grenaillage vibratoire est capable de générer des intensités Almen comprises entre 0.047 et 0.2 mmA. La deuxième partie a présenté la caractérisation de l'intégrité de la surface de l'acier cémenté E16NCD13 après le traitement de grenaillage vibratoire en termes de rugosité de surface, de contraintes

résiduelles de compression et de microdureté. Ils ont été mesurés et évalués après traitement sous trois intensités différentes (0.1, 0.15 et 0.2 mmA) et différentes conditions de traitement. La troisième partie a exposé une étude comparative des effets du grenaillage vibratoire et du grenaillage conventionnel sur l'intégrité de la surface de l'acier cémenté E16NCD13 en termes de rugosité de surface, de contraintes résiduelles de compression et de microdureté aux trois mêmes intensités 0.1, 0.15 et 0.2 mmA.

Ces expériences ont montré que le grenaillage vibratoire est capable d'améliorer le fini de surface de l'acier cémenté E16NCD13. Par exemple, il peut diminuer la rugosité de surface de 0.19 μm à 0.08 μm à des intensités Almen élevées. L'évolution de la rugosité de surface dépend de l'intensité Almen et des paramètres de la machine. Le procédé de grenaillage vibratoire a introduit une couche de contraintes résiduelles de compression, dont l'amplitude varie dans la plage de [-550 MPa, -845 MPa] et la profondeur varie dans la plage de [128 μm, 170 μm], en fonction des intensités et des paramètres de traitement. La microdureté de surface a été légèrement augmentée de 750 $\pm$ 30 HV à 850 $\pm$ 15 HV pour une intensité Almen de 0.2 mmA. Les paramètres de la machine n'ont aucun effet sur la microdureté. Comparé au grenaillage conventionnel, le grenaillage vibratoire a permis d'obtenir un meilleur fini de surface à la même intensité Almen. Cependant, à l'intensité Almen de 0.1 mmA avec la condition de traitement [28 cm - 17.5 Hz], le grenaillage vibratoire n'a pas été capable de réduire la rugosité de surface de l'acier traité en le comparant avec le grenaillage conventionnel. Le grenaillage vibratoire a également induit des contraintes résiduelles de compression maximales plus profondes, mais plus faibles. De plus, le grenaillage vibratoire a augmenté la microdureté de la surface du matériau traité alors que le grenaillage conventionnel n'a pas eu d'effet sur lui. Toutes ces interprétations permettent de conclure que le grenaillage vibratoire et le grenaillage conventionnel pourraient produire des résistances à la fatigue de l'acier cémenté E16NCD13 comparables. En outre, le grenaillage vibratoire pourrait améliorer la productivité industrielle en combinant deux procédés de traitement de surface en un seul.

ABSTRACT

Vibratory peening is an alternative process that aims to replace the shot peening and the vibratory finishing processes. It produces compressive residual stresses comparable to those obtained by shot peening but with much better surface finish, which is believed to enhance the fatigue life of the treated part. It is also believed to improve the industrial productivity by combining the shot peening and the vibratory finishing steps into one single process. Athough there are available studies on this process, no fundamental and physical works presenting the generated properties improvement were presented.

This study is part of a project that aims to demonstrate the beneficial effects of advanced surface treatment technologies on some aerospace materials which was a collaboration between Polytechnique Montréal, Safran Tech France and Aerospace and Technology Center Longueuil (CTA). This work focused on calibrating the vibratory peening machine and identifying its operation parameters limits. It involves also the study of the effect of vibratory peening on the surface integrity properties of the cemented steel E16NCD13 in terms of surface roughness, compressive residual stresses and microhardness. The surface integrity modifications produced by vibratory peening were compared to shot peening at similar Almen intensities.

The literature review showed that the Almen intensity, the processing time, the amplitude, the frequency, the media mass and the part position, etc. are the key parameters of the vibratory peening process. The first part of this study presented the relationship of the operation parameters, such as: media mass, eccentric weights, frequency, pressure, media height above the part, part position and lubrication rate with the amplitude of the vibratory peening machine and Almen intensity through design of experiments (DOE) techniques. The results showed that the vibration amplitude of the machine is mainly controlled by the eccentric weights on the rotating shafts, the rotational frequency of the rotating shafts, the media height above the part, and the Almen intensity is mainly influenced by the eccentric weights. The DOE results showed that the vibratory peening machine is able to generate Almen intensities ranged between 0.047 and 0.2 mmA. The second part presented the characterization of the surface integrity of the cemented steel E16NCD13 after vibratory peening in terms of surface roughness, compressive residual stresses and microhardness. They were measured and evaluated after treatment under three different intensities (0.1, 0.15 and 0.2 mmA) and different process conditions. The third part carried a comparative study of the effects of

vibratory peening and shot peening on the surface integrity of the cemented steel E16NCD13 in terms of surface roughness, compressive residual stresses and microhardness at the same three intensities 0.1, 0.15 and 0.2 mmA.

These experiments showed that vibratory peening is able to improve the surface finish of the cemented steel E16NCD13. For example it can decrease the surface roughness from 0.19 μm to 0.08 μm at high Almen intensities. The evolution of surface roughness depended on Almen intensity and on the machine parameters. The vibratory peening process introduced a layer of compressive residual stresses, where its magnitude varies in the range of [-550 MPa, -845 MPa] and its depth in the range of [128 μm, 170 μm], depending on the intensities and processing parameters. The surface microhardness was slightly increased from 750 $\pm$ 30 HV to 850 $\pm$ 15 HV at Almen intensity of 0.2 mmA and the machine parameters have no effect on it. Compared to shot peening, vibratory peening induced better surface finish a the same Almen intensity. However, at Almen intensity of 0.1 mmA with the treatment condition [28 cm - 17.5 Hz], vibratory peening was not able to reduce the surface roughness of the treated steel when compared to shot peening. Vibratory peening induced also deeper, but smaller maximum compressive residual stresses. Moreover, vibratory peening increased the surface microhardness of the treated material while shot peening had no effect on it. All these interpretations allow to conclude that the vibratory peening and shot peening could produce similar fatigue lives of treated E16NCD13 steel. Besides, vibratory peening could improve the industrial productivity by combining two surface treatment processes into one.

TABLE OF CONTENTS

LIST OF TABLES

LIST OF FIGURES

LIST OF APPENDICES

CHAPTER 1 INTRODUCTION

Since 2016, Polytechnique Montréal and Safran Tech, France, are committed to a research project that aims to demonstrate the potential beneficial effects of an advanced surface treatment called vibratory peening on the surface integrity of aerospace materials including the cemented steel E16NCD13, which is used in Safran's gearboxes and gears. The project's objective is to demonstrate that vibratory peening is likely to lead to more durable aerospace parts, to increase productivity and to lower costs, making the aerospace industry more competitive.

Shot peening is a surface treatment used to improve the fatigue properties of materials by retarding the initiation and propagation of short cracks [2]. However, the surface roughness induced by shot peening creates a stress concentration which tends to reduce the component's fatigue life [3]. Additional surface finishing processes, like vibratory finishing, are often required to reduce the generated surface roughness and provide better surface finish [4].

Vibratory peening is an alternative process that combines the beneficial effects of shot peening and vibratory finishing [5]. It could therefore improve fatigue life and reduce the number of processes that a machined part must undergo before being put into service.

E16NCD13 is a cemented low alloy steel used in aircraft components like gears and gas turbine engines [5]. These components are submitted to contact and rotary bending fatigue during their applications, which requires a surface treatment to enhance their fatigue resistance.

My thesis aims to assess the potential of vibratory peening to replace shot peening and vibratory finishing processes. This assessment is achieved by studying the effects of vibratory peening on the surface integrity, in terms of surface roughness, residual stresses, and hardness, of the cemented steel alloy E16NCD13 and comparing them to those obtained after shot peening at similar Almen intensities.

This research project was done in collaboration between Polytechnique Montréal, Safran Tech and CTA, a Collegial Center for Technology Transfer, where the vibratory peening machine was installed. This project was financed by Safran Tech and Natural Sciences and Engineering Research Council of Canada (NSERC).

This document is divided into 4 chapters and organized as follows: Chapter 2 presents and synthesises the literature related to the project. Chapter 3 sets the objectives for my project. Chapter 4 describes the materials and methodology developed to reach the objectives. Chapter 5 describes the results obtained from the experimental work during the project and the project's general conclusions are presented in Chapter 6.

CHAPTER 2 LITERATURE REVIEW

2.1 Cemented steel E16NCD13

The studied material is cemented steel E16NCD13 used in Safran's engines gearboxes and gears. This alloy was selected for the vibratory peening study since the surface finish of parts made of this alloy has a strong effect on contact fatigue. In addition, recent studies showed that vibratory peening produced significant residual stresses that could enhance the alloy's fatigue life.

2.1.1 Case hardening

The case hardening treatment consists in diffusing carbon into the surface of low carbon steel followed by quenching treatment after machining as illustrated in Figure 2.1(a) [6]. The process aims to improve the contact and bending resistance by hardening the surface, increasing the tensile strength of the cemented steel and introducing a compressive residual stress layer [7].

Li et al. [7] developed a finite element model to study the effect of case depths (CD) on AMS 6308 cemented steel residual stresses. The CD was defined as the distance from the surface of the part to the depth where the hardness is of 550 HV as shown in Figure 2.1(b) [8]. At a case depth of 0.5 mm, the surface compressive residual stress was of -1050 MPa and increased to -1250 MPa for a CD of 1.5 mm. Besides, the depth of compressive residual stresses increased from 0.7 mm for a CD of 0.5 mm to 2 mm for a CD of 1.5 mm. Therefore,

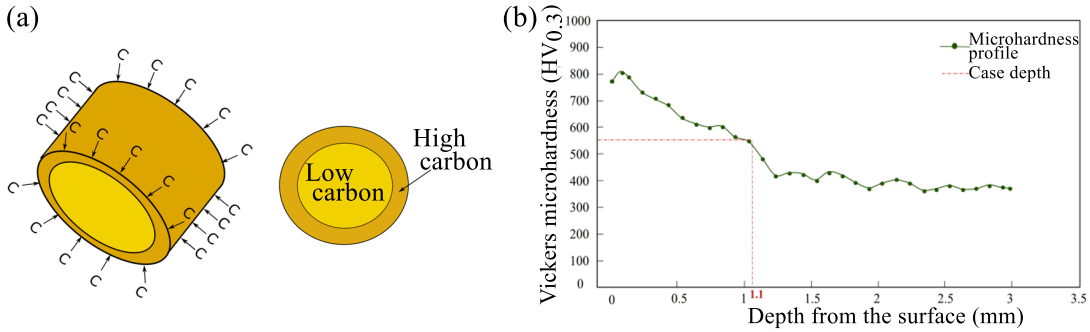

Figure 2.1 *Cemented steel illustration. (a) The case hardening consists in diffusing carbon amount into the surface of low carbon steel. (b) The case depth of cemented steel is the distance for the surface to the depth where the hardness is of 550 HV.*

the magnitude and the depth of residual stresses of AMS 6308 steel depended mainly on the CD.

2.1.2 Properties of cemented steel E16NCD13

E16NCD13 is a low alloy steel that can be cemented and used in various mechanical and aerospace industry parts. Its chemical composition is given in Table 2.1 [9]. Table 2.2 lists the mechanical properties of as-received cemented steel E16NCD13 specimen having dimensions of $79.9 \times 18.9 \times 8$ mm^3 [5]. The surface hardness of the cemented steel after case hardening, quenching and tempering can achieve 700 HV. It is characterized by a good toughness of the cemented layer, good mechanical characteristics and high fatigue resistance [10].

2.2 Shot peening

Shot peening consists in impacting a metal component with hard shot, at high velocity. The large number of impacts induces local plastic strains leading to a localised sub-surface layer of compressive residual stresses and a work hardening, as schematized in Figure 2.2. These effects delay the initiation and propagation of short cracks [2]. However, the detrimental effect of this process is the increased surface roughness due to the dimples created by the impact between the material and the media surfaces. The surface roughness greatly influences the fatigue performance of the treated workpiece [3].

The operating parameters of shot peening are air pressure, peening time, impact angle, nozzle diameter, shot material, shot velocity, media-flow rate, etc [11]. The controlling parameters that define the efficiency of the shot peening process are the Almen intensity and the coverage [12].

2.2.1 Controlling parameters

Almen intensity characterizes the kinetic energy transferred from the shot to the peened parts during the peening process [12]. It is obtained by measuring the deflections of standardized SAE 1070 steel strips, called Almen strips, that are shot peened for different processing

Table 2.1 *Chemical composition of cemented steel E16NCD13 (ISO 683-17) [9].*

Element	Fe	C	Mn	Si	Cr	Ni	Mo	Cu	P	S
Wt%	Balance	0.16	0.46	0.20	1.02	3.00	0.26	0.13	0.008	0.010

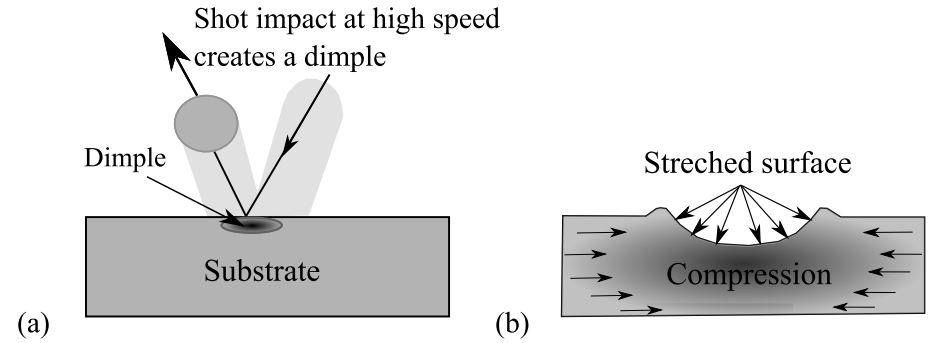

Figure 2.2 *Shot peening illustration. (a) The impact of the high speed media creates a dimple. (b) Stretched surface induced by shot peening creating a plastic deformation counterbalanced by residual compressive stresses.*

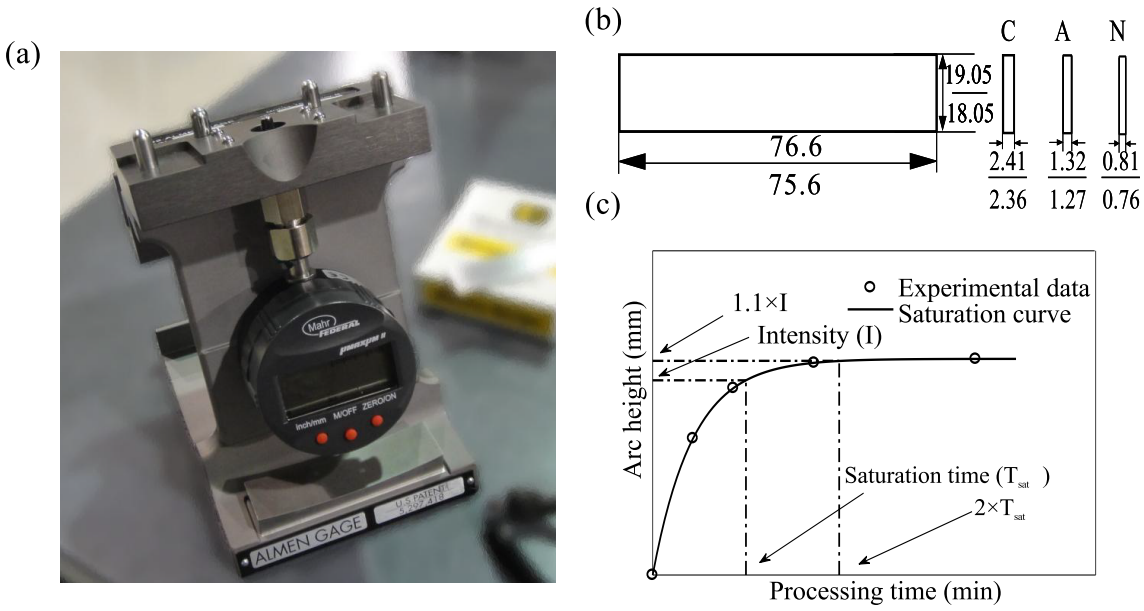

Figure 2.3 *Almen intensity computation and Almen strips. (a) The arc height of Almen strips measured with a standardized Almen gauge to get the Almen arc height. (b) The dimensions of N, A and C Almen strips as per SAE J442 [14]. (c) The saturation curve is defined as the arc height (mm) as a function of the processing time (min) as per SAE J443 [13]. The saturation time corresponds to the first point where doubling the peening time produces no more than a 10 % rise in arc height. The Almen intensity is the arc height at the saturation time* T_{sat}.

Table 2.2 *Mechanical properties of a normalized, annealed, case hardened and gas quenched cemented steel E16NCD13 specimen having dimensions of 79.9 × 18.9 × mm^3 (ISO 683-17) [5]. Young's modulus (E), Poisson's ratio (ν), density (ρ), yield stress at 0.2% ($R_{0.2}$), ultimate stress (R_m), surface hardness and bulk hardness are as given.*

Property	E [GPa]	ν [ ]	ρ [g.cm^{-3}]	$R_{0.2}$ [MPa]	R_m [MPa]	Surface hardness [HV]	Bulk hardness [HV]
Value	210	0.28	7.85	1 000	1 350	750	400

times, with a standardized Almen gauge showed in Figure 2.3 (a). The thickness of the Almen strip depends on the anticipated intensity and is classified into three types: N, A, and C. The corresponding thickness are of [0.76-0.81], [1.27-1.32] and [2.36-2.41] mm for strips N, A and C, respectively, as shown in Figure 2.3(b) [14]. As specified by standard SAE J443 [13], a saturation curve is defined as the arc height as a function of the peening time. The saturation time T_{sat} corresponds to the first point where doubling the peening time produces no more than a 10% rise in arc height. The Almen intensity is the arc height at the T_{sat}, as illustrated in Figure 2.3 (b) [5].

Media type [15], media diameter [16, 17], media velocity [18], peening pressure [16, 17], etc., all influence Almen intensity. Almen intensity increases with the increase of media size, media hardness, media velocity and peening pressure.

Peening coverage is defined by SAE J2277 [19] as the ratio of the area covered by indentations to the total peening area, expressed in percentage. A coverage of 98% is defined as full coverage or 100% coverage. A coverage greater than 100% corresponds to multiples of the time required to reach full coverage (e.g., a coverage of 200% means that the part has been peened for twice the time required to reach a coverage of 98%).

2.2.2 Optimization of shot peening parameters

Almen intensity is the most important controlling parameter that is used to characterize the efficiency of shot peening. However, since it is influenced by other process parameters, numerous studies investigated the relationship between Almen intensity and other parameters using a Design Of Experiments (DOE) method. The DOE method is a statistical approach for defining the relationship between the parameters and responses [20]. This design consists in involving an empirical model to relate the response with the input parameters and it is

described as follow:

$$y = \sum_i \beta_i \chi_i + \epsilon, \tag{2.1}$$

where y is the response, χ_i are the input parameters, β_i are the coefficients that will describe the statistical significance of the input parameters on the response and ϵ is the experimental error. The last term is estimated by replicating and randomizing the tests [21]. The objective of DOE is to define the relationship between the response and the input parameters with a minimal number of experiments. However, the fully randomized design is time-consuming. Consequently, split plot is a partially randomized design used when some parameters are harder to manipulate than others. Nevertheless, this may affect the accuracy of ϵ value [21].

Unal [17] analysed the effect of shot peening air pressure, shot diameter and peening time on the arc height using response surface methodology (RSM). RSM is DOE where the response is affected by some parameters and the purpose is to optimize the response [21]. An analysis of variance (ANOVA) was performed to determinate the statistical significance of each parameter on the Almen intensity obeying:

$$A = 2101 - 0.029 \times t - 0.0313 \times s - 0.044 \times p + 0.01 \times t \times s + 0.06 \times t \times p + 0.07 \times s \times p, \tag{2.2}$$

where A (mm) is the arc height, t (s) is the peening time, s (mm) is the shot diameter and p (kPa) is the air pressure. The equation (2.2) reveals that the pressure (p) and its interaction with the shot diameter ($p \times s$) and with the peening time ($p \times t$) are the most important factors that influence Almen intensity.

Bucior et al. [22] investigated the effect of processing time and air pressure on Almen intensity using DOE method. They revealed that Almen intensity increased with the increase of air pressure.

2.2.3 Effect of shot peening on cemented steel surface integrity

Surface roughness

The most common roughness parameters are R_a, R_t, R_{sk} and R_{ku}. They are computed according to ISO 4287 standard from measured profiles as [24]:

- Average roughness R_a in Figure 2.4(a) is an arithmetical mean deviation of the rough-

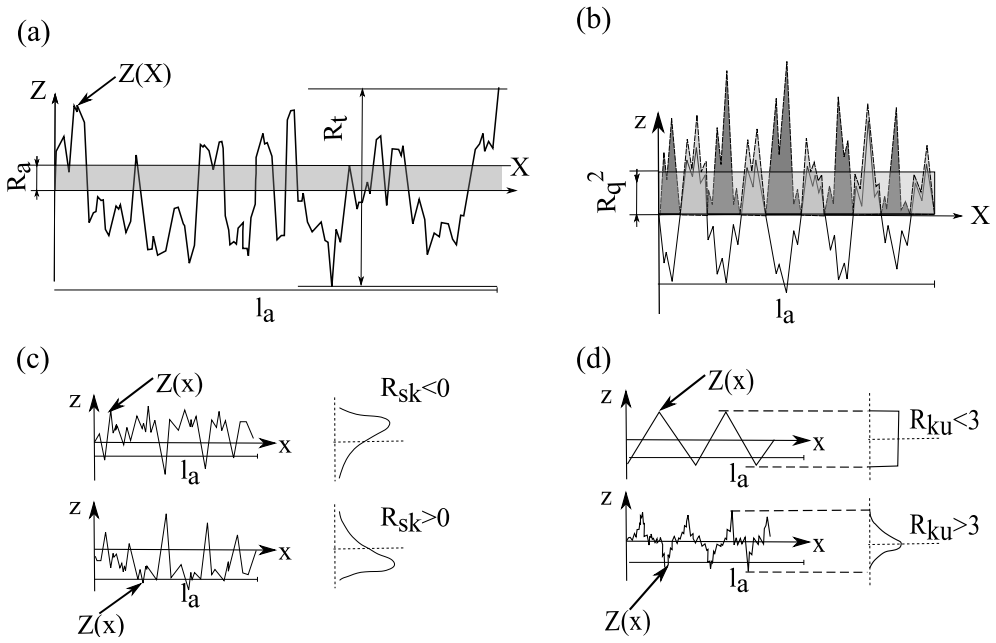

Figure 2.4 *Schematization of surface roughness parameters. (a) Average roughness R_a is the arithmetical mean deviation of the roughness, $Z(x)$ is the height of the profile at position x, and total height R_t is the height between the deepest valley and the highest peak on the evaluation length. (b) The root mean square value of ordinate values R_q.(c) Skewness roughness R_{sk} is the cube of the root mean square deviation. (d) Kurtosis roughness R_{ku} is the fourth power of the root mean square deviation [23].*

ness as:

$$R_a = \frac{1}{l_a} \int_0^{l_a} |Z(x)| \, \mathrm{d}x, \tag{2.3}$$

where $Z(x)$ is the height of the profile at position x, l_a is the measured length. It provides a general description of height variations.

• Roughness parameter R_t, as shown in Figure 2.4(a), is the total height between the deepest valley and the highest peak on the evaluation length.

$$R_t = \max_{l_a} Z(x) - \min_{l_a} Z(x), \tag{2.4}$$

• Skewness roughness R_{sk} is defined as the cube of the root mean square deviation to display the dimensionless cube of the sampling length $Z(x)$,

$$R_{sk} = \frac{1}{R_q^3} \frac{1}{l_a} \int_0^{l_a} Z^3(x) \mathrm{d}x, \tag{2.5}$$

where R_q represents the root mean square value of ordinate values within the definition area, as shown in Figure 2.4(b). R_{sk} is equivalent to the standard deviation of heights. It expresses the symmetry of peaks and valleys using the average line as the center. $R_{sk} < 0$ means that the surface is made up of deep valleys and low peaks, otherwise the surface is made up of high peaks and shallow valleys as presented in Figure 2.4(c).

• Kurtosis roughness R_{ku} uses the fourth power of the root mean square deviation to display the dimensionless fourth power of the sampling length $Z(x)$ as:

$$R_{ku} = \frac{1}{R_q^4} \frac{1}{l_a} \int_0^{l_a} Z^4(x) \mathrm{d}x, \tag{2.6}$$

R_{ku} represents the probability density sharpness of the profile. If $R_{ku} > 3$, the height distribution is sharp, otherwise it is flat, as shown in Figure 2.4(d).

Nordin et al. [1] investigated the effect of shot peening Almen intensity on the surface roughness of SS 92506 steel. The Almen intensity ranged between 0.22 mmA and 0.49 mmA and the used media was a cut wire with a size of 0.7 mm. The measured roughness parameter was the arithmetic mean deviation R_a. For a given coverage of 200%, R_a increased with the increase of Almen intensity. The surface roughness increased from 0.5 ± 0.02 μm (not peened)

to 0.65 ± 0.05 μm and 0.86 ± 0.05 μm for Almen intensity of 0.22 mmA and 0.49 mmA, respectively. Chang et al. [25] investigated the effect of shot peening on the surface roughness of 9310 steel alloy for Almen intensities between 0.1 mmA and 0.3 mmA using S70 cast steel shot with a coverage of 200%. Their study showed that peening at intensities of 0.1 mmA and 0.3 mmA yielded an increase of R_a from 0.76 μm to 1.5 μm and 4.4 μm, respectively. To conclude, the surface roughness of cemented steel increases with the increase of Almen intensity, which can be explained by the fact that higher intensity induces higher velocity and deeper impact as a result.

Nordin et al. [1] studied also the effect of the coverage on the surface roughness of SS92506 steel. For a given Almen intensity of 0.34 mmA, the coverage varied from 100% to 400%. The R_a decreased with the increase of the coverage. It increased from 0.5 ± 0.02 μm to 0.75 ± 0.03 μm for a coverage of 100% and then it decreased continuously by increasing the coverage to reach 0.68 ± 0.08 μm at a coverage of 400%. The reason of this evolution is that for the first passes, the shot creates deep peaks and valleys that increase the surface roughness and creating a work hardening and compressive residual stress at the same time. The further media passes were not able to create deeper dimples and they come therefore to polish the surface and smash the previous peaks. The R_a was then decreased [1].

The authors investigated also the effect of shot peening Almen intensities on the surface topography of SS92506 steel under a coverage of 200%. Figure 2.5 shows that shot peening under an Almen intensity of 0.22 mmA removed completely the machining marks and maintaining the same level of surface roughness height as the non treated surface. Shot peening with Almen intensity of 0.49 mmA managed also to erase the machining marks but the surface roughness height was higher than of non treated surface. It increased from 6.21 μm to 7.99 μm. This consequence is beneficial to the fatigue strength since it helps in decreasing the fatigue initiation sites related to higher stress concentration factors associated with machined marks at the surface [1].

Compressive residual stresses

Figure 2.6 [26] shows a typical residual stresses profile in a shot peened cemented steel gear. The shot peening conditions were not provided. The surface compressive residual stress σ_{sur} were about -828 MPa and the maximum compressive residual stresses σ_{max} of -1379 MPa were achieved at the depth of the maximal stresses $d_{\sigma,max}$ of 0.03 mm. $d_{\sigma,c}$ is the depth of influence and it corresponds to the depth where the compressive residual stresses remain stable. A stabilized compressive residual stress of -276 MPa, which extended deeper than

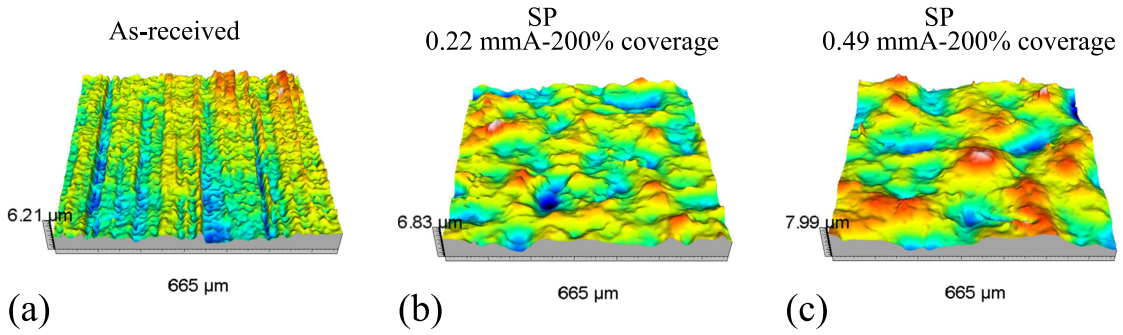

Figure 2.5 *Surface topography of SS92506 steel before and after shot peening. (a) As-received, (b) shot peened under 0.2 mmA and 200% coverage (c) and shot peened under 0.49 mmA and 200% coverage. Shot peening erased the machining marks. Higher Almen intensity leads to higher surface roughness [1].*

200 μm, corresponded to the influence of case hardening before shot peening [5].

Ho et al. [27] studied the effect of shot peening on the residual stresses of cemented steel 18 CrNiMo7-6 alloy. Two Almen intensities of 0.25 mmA and 0.45 mmA, and two cast steel shot diameters of 0.6 mm and 0.3 mm, were investigated. The coverage was of 200% for all peening conditions. For shot peening with a media diameter of 0.6 mm, when the Almen intensity increased from 0.25 mmA to 0.45 mmA, the σ_{sur} increased from -400 MPa to around -500 MPa and σ_{max} increased from -900 MPa to -980 MPa, respectively. An increase of $d_{\sigma,c}$ from 0.2 mm to 0.5 mm was observed when increasing Almen intensity from 0.25 mmA to 0.45 mmA. $d_{\sigma,max}$ was not affected by Almen intensity evolution. This is related to the higher velocity induced by the increase of the Almen intensity which produces more kinetic energy and deeper plastic deformation [27].

For the same Almen intensity of 0.25 mmA, when the media diameter increased from 0.3 mm to 0.6 mm, the σ_{sur} decreased from around -580 MPa to -400 MPa and the σ_{max}, $d_{\sigma,0}$ and $d_{\sigma,max}$ were almost constant. The explanation of this effect is that the contact of the treated material with bigger media is larger generating smaller contact pressure, with a larger impact surface. As a result, the plastic deformation is reduced inducing a decrease in the compressive residual stress [27]. Therefore, the residual stresses distribution on shot peened cemented steel 18 CrNiMo7-6 depended on the combination of Almen intensity, media diameter and shot velocity.

Guagliano et al. [28] numerically analysed residual stress profiles of cemented steel 39NiCrMo3 after shot peening for different shot sizes and velocities. The analysis was carried out con-

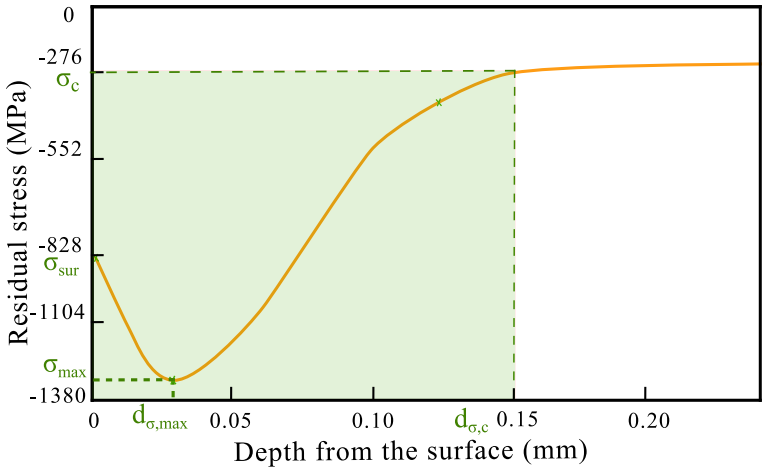

Figure 2.6 *Typical compressive residual stress profile of cemented and shot peened steel. The shot peening conditions were not provided.* σ_{sur} *corresponds to the surface compressive residual stress,* σ_{max} *corresponds to the maximum compressive residual stress,* $d_{\sigma,max}$ *is the depth of the maximal stress and* $d_{\sigma,c}$ *is the depth of influence, which is defined as the depth of compressive residual stresses generated by shot peening, The compressive residual stress* σ_c *(-276 MPa), which extends deeper than 0.2 mm, corresponds to the influence of the case hardening before shot peening [26].*

sidering a constant Almen intensity of 0.3 mmA and coverage of 200%. Increasing the shot diameter from 0.3 mm to 1 mm led to an increase of $d_{\sigma,c}$ from 0.1 mm to 0.22 mm and $d_{\sigma,max}$ from 0.6 mm to 1 mm. Increasing the media velocity from 40 m/s to 100 m/s for a diameter of 1 mm led to an increase of $d_{\sigma,c}$ from 0.22 mm to 0.35 mm and $d_{\sigma,max}$ from 0.5 mm to 1 mm. The shot size and velocity seems not to have a pronounced effect on σ_{sur} and σ_{max}. This suggests that peening a surface of cemented steel with large shot at higher velocities led to deeper profiles due to the higher Hertzian pressure. This phenomenon can be expected for vibratory peening. As a conclusion, the residual stresses distribution on cemented steel depended on the combination of Almen intensity, shot diameter and shot size.

Microhardness

Trung et al. [15] shot peened AISI 4340 specimens at an Almen intensity of 0.275 mmA (11 A), with 0.6 mm diameter steel balls with a hardness of 500 ± 30 HV. The authors found that the hardness increased to 440 ± 11 HV at the surface and decreased progressively to the original material hardness (325 ± 12 HV) after 300 μm. This cold working is due to high strain rate impact during the shot peening process.

Nordin et al. [1] compared the microhardness profiles of SS92506 steel before and after shot

peening with three different Almen intensities (0.22 mmA, 0.34 mmA and 0.49 mmA) under a coverage of 200% and a cut wire media with a size of 0.7 mm and hardness of 656-774 HV. The surface microhardness increased from 716 ± 12 HV to comparable values around 870 ± 2 HV for all the intensities. The microhardness below the surface increased with the increase of Almen intensity.

Ho et al. [27] studied the microhardness profiles evolution as a function of shot peening parameters. When peening cemented steel 18CrNiMo7-6 with a steel media having a diameter of 0.6 mm, increasing the Almen intensity from 0.25 mmA to 0.45 mmA induced a rise of surface microhardness by 6.3% and 9.5%, respectively. For a constant Almen intensity of 0.25 mmA, microhardness raised by 5.2% and 6.3% for 0.3 mm and 0.6 mm shot, respectively.

Renaud et al. [30] quantified the impact of shot peening, using an Almen intensity of 0.15 mmA and 0.4 mm diameter steel media having a hardness of 700 HV, on the transformation of residual austenite into martensite on 29MnCr cemented steel. The study showed that the martensite contents on the surface increased by 35% after shot peening. This transformation could be associated to the increase of surface microhardness after shot peening in most cemented steels.

To sum up, shot peening increases the surface microhardness of cemented steel and has no effect on the CD. The increase of Almen intensity and media diameter enhances the increase of surface microhardness. This evolution is mainly related to the work hardening produced by shot peening. The microstructural changes in the cemented layer associated to the transformation of the retained austenite to martensite could be also another reason of the microhardness increase.

2.3 Vibratory finishing

Vibratory finishing is a polishing process consisting in inserting a part into an oscillating bowl filled with abrasive media as illustrated in Figure 2.7. Polishing is achieved by the interactions between the part and the media surfaces. The bowl is attached to springs and rotating shafts with eccentric masses. The vibration movement is provided by the rotation of the shafts [29]. The vibration amplitude, the frequency and the media mass and type are the key parameters of the process. Moreover, the choice of the level of each parameter depends on the desired effect on the treated material [31].

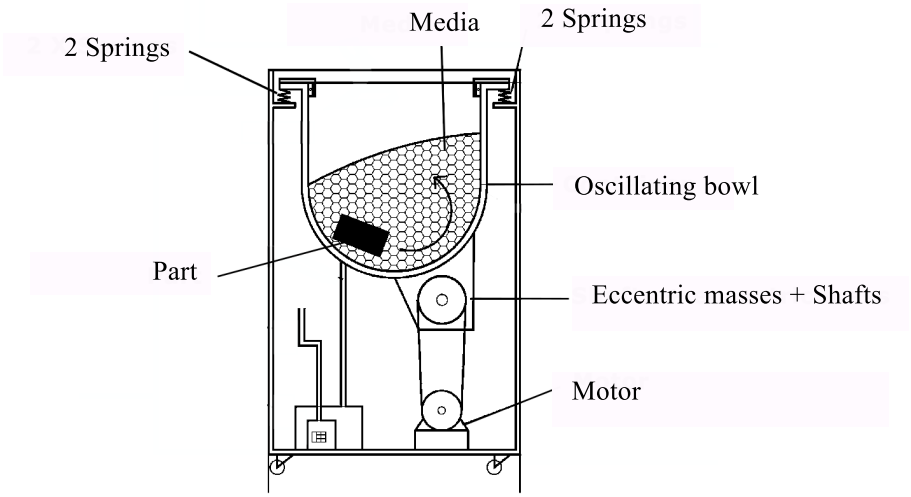

Figure 2.7 *A Schematic of vibratory finishing. The oscillating bowl full of media is attached to springs and a shaft with an eccentric mass manipulated by a motor, the vibration movement is provided by the rotation of the shaft around the component [29].*

2.3.1 Controlling parameters

Vibration amplitude is controlled by the eccentric weights which are mounted on the rotating shafts [32, 33]. It depends also on the media mass in the tub and increasing the media mass reduces the vibration amplitude [34, 35]. The vibration amplitude also depends on the springs stiffness [36]. However, the media type doesn't have a significant effect on the amplitude [34, 37].

Frequency is controlled by the motor speed rotation [38]. Sofran et al. [39] and Pandiyan et al. [38] found that it was the most important parameter that influences the vibratory finishing process performance in term of surface finish and that the high frequency led to the best surface finish improvement in the least time.

Media: A variety of media shapes are used in vibratory finishing such as pyramids, triangles, cones and spheres while the size is lower than 25 mm. The media size, material and roughness affected greatly the efficiency of vibratory finishing in terms of surface finish since they influenced the interaction between the workpiece and the media surfaces [38].

2.3.2 Effect of vibratory finishing on aerospace alloys surface integrity

Surface roughness

Wang et al. [40] studied the correlation between the conditions of vibratory finishing and the surface roughness of AA1100-O aluminum alloy having an initial surface roughness R_a of 0.4 μm. Vibratory finishing was applied using 9 mm spherical ceramic media with two different roughness values (15.4 $\pm$ 6.3 μm and 13.8 $\pm$ 2.3 μm) and under three different lubrication conditions (dry, water-wet and detergent). For all lubrication conditions, the measured roughness of the treated part increased with the increase of the media roughness. The maximum surface average roughness R_a of 2.3 μm was obtained under the dry condition and with the media of surface roughness 15.4 $\pm$ 6.3 μm.

Domblesky et al. [41] studied the effect of vibratory finishing on the surface roughness on AISI 1018 steel and Al6061 aluminum alloys using Al_2O_3 ceramic rough media for a processing time of 6 hours and a bowl acceleration of 27.4 m/s^2. The surface hardness of the treated steel and aluminium alloys were of 180 HV and 112 HV, respectively. The harder steel material achieved better surface finish (R_a = 54 μm) than the softer aluminium workpiece (R_a = 85 μm). However the initial roughness of both materials were unknown.

Microhardness

Wang et al. [40] established a correlation between the conditions of vibratory finishing and the resulting hardness on AA1100-O aluminum alloy. The AA1100-O specimens were treated by spherical ceramic media with three different [media size - media surface roughness] couples ([7 mm - 17.5 $\pm$ 4.1 μm], [9 mm - 15.4 $\pm$ 6.3 μm] and [11 mm - 16.2 $\pm$ 4.7 μm]). It was found that increasing the processing time for different media and lubrication conditions (dry, water-wet and detergent) increased the hardness of AA1100-O. Besides, the surface hardness measurements showed that the maximum hardness (60 HV) was achieved under the dry condition and with media sizes of 11 mm. Moreover, for a processing time of 40 min, media size of 9 mm and under the dry condition, the media with a roughness of 15.4 $\pm$ 6.3 μm induced a hardness of 48 HV, while a hardness of 35 HV was achieved with the media roughness of 13.8 $\pm$ 2.3 μm. Therefore, the media with the rougher surface produced higher hardness in the treated specimen. In conclusion, the processing time, the lubrication condition, the media size and the media roughness have significant effects on the resulting hardness of vibratory finished materials.

2.4 Vibratory peening

Vibratory peening combines shot peening and vibratory finishing into one process. It produces a sub-surface compressive residual stress field similar to that obtained by shot peening, with a much better surface finish, which is believed to enhance the fatigue life of treated parts. Vibratory peening consists in fixing a part into a container filled with media, having diameters ranging from 2 mm to 6 mm, as shown in Figure 2.8.

2.4.1 Controlling parameters

Ciampini et al. [29] used an Almen system to characterize vibratory peening using aluminium Almen strips with carbon steel media with a diameter of 6.3 mm. Different processing times and impact velocities were used to investigate the efficiency of Almen system to describe vibratory peening performance. The authors found that for a constant processing time, increasing the impact velocities led to an increase of arc heights. Besides, for a given impact velocity, a longer treatment time led to a higher arc height. They concluded that the Almen system is appropriate to characterize the vibratory peening process.

Canals et al. [5] analysed the effect of vibratory peening parameters frequency and media mass on the Almen intensity. A mix of steel bearing shot in equal proportions with diameters of 3.18 mm, 6.35 mm and 7.76 mm was used. For a constant media mass of 792 kg, the increase of the frequency from 23 Hz to 30 Hz led to an increase of the Almen intensity from 0.12 mmA to 0.25 mmA, which corresponds to the intensities range attainable with this process during this study.

Sangid et al. [42] investigated the effect of treatment time on arc height of N strips, using ceramic media with sides of 6.35 mm, by plotting the saturation curve as for Figure 2.3, for processing time of 15, 30, 45, 60, 75 min. The saturation point was found at a treatment time of 60 min, which means that for constant conditions, Almen intensity get saturated for certain processing time.

To summarize, Almen intensity is appropriate to describe the vibratory peening process. Almen intensity increases with the increase of processing time, impact velocities and frequency.

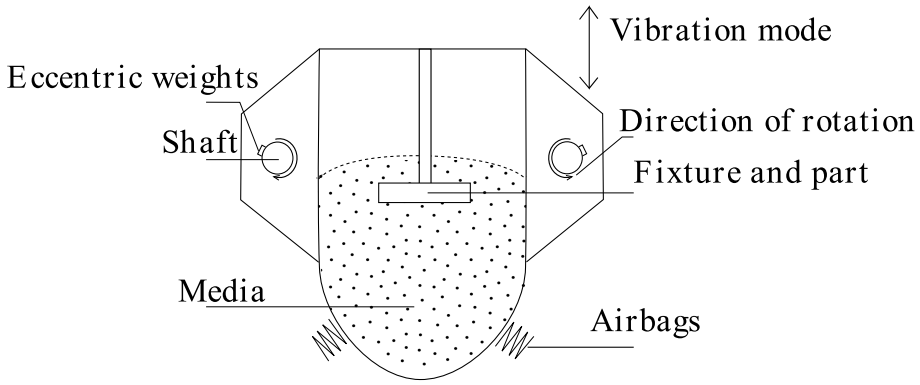

Figure 2.8 *A typical mechanism of a vibratory peening machine. The rotating shafts induce the tub's vibration. The movement of the media around the part induce the peening and finishing effects [5].*

2.4.2 Effect of vibratory peening on cemented steel surface integrity

Surface roughness

Canals et al. [5] studied the effect of vibratory peening processing time and Almen intensity on cemented steel E16NCD13 surface roughness. For a constant Almen intensity of 0.12 mmA, R_a decreased with the increase of processing time and reached a stable value of 0.4 μm at $2T_{sat}$. This was valid also for Almen intensities of 0.18 mmA and 0.25 mmA. However, the Almen intensity had an insignificant effect on R_a after a processing time of $2T_{sat}$.

Compressive residual stresses

Canals et al. [5] investigated also the effect of vibratory peening Almen intensity on the compressive residual stress field of cemented steel E16NCD13 at a processing time of $2T_{sat}$. The authors found that the σ_{max} and the $d_{\sigma,0}$ increased with the increase of Almen intensity. The increase of Almen intensity from 0.12 mmA to 0.25 mmA led to an increase by 345% of σ_{max} and $d_{\sigma,c}$ deepening by 135%.

For a constant Almen intensity of 0.18 mmA, a frequency of 47 Hz, the increase of processing time from T_{sat} to $2T_{sat}$ generated a rise by 6% and 66% of σ_{max} and $d_{\sigma,c}$, respectively [5]. An increase of a frequency from 25 Hz to 47 Hz, for an Almen intensity of 0.18 mmA, produced an increase of 9% and 24% of σ_{max} and $d_{\sigma,c}$, respectively [5].

To sum up, the study on the effect of vibratory peening on residual stress field revealed

that higher Almen intensity, higher processing time, and higher frequencies led to deeper and larger compressive residual stress field.

Hardness

Canals et al. [5] compared the hardness profiles of cemented steel E16NCD13 before and after vibratory peening. For a mass of media of 792 kg and a peening time of T_{sat}, vibratory peening produced a slight increase in the surface hardness fom 720 HV to around 780 HV, for different intensities (0.12 mmA, 0.18 mmA and 0.25 mmA) within the first 70 μm from the surface. For an Almen intensity of 0.18 mmA, an increase of the surface hardness up to 820 HV was observed for a media mass of 555 kg.

2.5 Comparison of the effect of shot peening, vibratory finishing and vibratory peening on surface integrity and fatigue life

2.5.1 Effect of shot peening and vibratory peening on surface integrity and fatigue life

Kumar et al. [43] investigated the effects of shot peening and vibratory peening on Ni-based superalloy (Udimet 720Li) in terms of surface roughness, compressive residual stresses and micro hardness. Udimet 720Li specimens were shot peened with cast steel media of 0.29 mm diameter and were vibratory peened by steel media with a dimension of 5 - 7 mm and with a vibration amplitude of 5.5 mm. Both processes were applied at the same Almen intensity of 0.1 - 0.12 mmA. Miao et al. [44] studied the effects of shot peening and vibratory peening on AA7050-T7451 aluminum alloy in terms of surface roughness, compressive residual stresses and high cycle fatigue (HCF) behavior. The media used in shot peening was ceramic Z425. The media used in vibratory peening was hard steel shot with diameters of 3 mm, 4.5 mm and 6 mm with an amplitude of 9 mm and a frequency of 50 Hz. Both processes were applied at the same Almen intensity of 0.3 mmA. Canals et al. [5] performed a comparative study on cemented steel E16NCD13 and Ti-6Al-4V titanium alloy to investigate the effects of shot peening and vibratory peening. Both alloys were vibratory peened with equal proportions mix of bearing steel media of 3.18 mm, 4.76 mm and 7.76 mm and shot peened with ASR130 steel media under iso Almen Intensity of 0.18 mmA. The results of both studies in terms of surface roughness, compressive residual stresses, microhardness and fatigue life will be presented in the following parts.

Surface roughness

Kumar et al. [43] found that the surface roughness increased from 0.01 μm to 0.71 μm for shot peening and to 0.26 μm for vibratory peening on Udimet 720Li. The surface roughness measurements from Miao's work [44] revealed that vibratory peening reduced the surface average roughness from about 1 μm to 0.75 μm, whereas shot peening increased the surface roughness to 6.56 μm for the AA7050-T7451 aluminum alloy. Canals et al. study [5] showed that the surface roughness is lower by 40 % and 82 % after vibratory peening, when compared to shot peening for cemented steel E16NCD13 and Ti-6Al-4V titanium alloy, respectively.

Compressive residual stresses

The residual stresses distributions on Udimet 720Li in Kumar's study [43] showed that the σ_{sur} was of -826 MPa after shot peening and of -640 MPa after vibratory peening. The σ_{max} was of -1094 MPa for shot peening and of -874 MPa for vibratory peening. The $d_{\sigma,c}$ was larger after vibratory peening (200 μm), when compared to that obtained from shot peening (140 μm). Miao's study [44] compared the residual stresses profiles of AA7050-T7451 aluminum alloy after shot peening and vibratory peening at the same Almen intensity. The σ_{sur} and σ_{max} were of -225 MPa and -300 MPa, respectively, for shot peening, and were of -150 MPa and -200 MPa, respectively, for vibratory peening. However, the $d_{\sigma,c}$ were 340 μm and 520 μm for shot peening and vibratory peening, respectively. Canals et al. [5] found that, at an Almen intensity of 0.18 mmA, for cemented steel E16NCD13, vibratory peening generated higher σ_{sur}, σ_{max} and $d_{\sigma,c}$ by 24%, 26% and 131%, respectively, when compared to shot peening. For Ti-6Al-4V titanium alloy, shot peening and vibratory peening provided similar residual stress profiles. The difference of compressive residual stresses distribution was explained by the different types of kinetic energies associated with each process, where the mechanism of plastic deformation, strain rate and strain gradient generation are different [43].

Microhardness

Kumar et al. [43] presented also the micro hardness generated by shot peening and vibratory peening. The average surface micro hardness of the as received specimen was 534 HV. It increased to 694 HV after shot peening and to 771 HV after vibratory peening. However, the rate of decrease following the depth is higher in shot peening than in vibratory peening. The micro hardness decreased rapidly to the original micro hardness within the first 150 μm for shot peening and persisted down to 250 μm for vibratory peening. Miao et al. [44] and Canals et al. [5] didn't present comparative microhardness measurements.

Fatigue life

Miao et al. [44] performed a comparative study between shot peening and vibratory peening to investigate their effects on the fatigue life of AA7050-T7451 aluminium alloy. They carried out HCF and low cycle fatigue (LCF) tests on AA7050-T7451 aluminium alloy specimens at maximum stresses of 310 MPa and 450 MPa, respectively, under a stress ratio of $R = 0.1$ and a frequency of 20 Hz. The results revealed that fatigue lives were similar for both processes in both domains and were about 250 000 cycles for HCF and about 20 000 cycles for LCF. The crack initiated from multiple surface locations under LCF and from subsurface under HCF. The failure modes were similar for shot peening and vibratory peening for the same fatigue domain.

To conclude, for both Udimet 720Li and AA7050-T7451 aluminum alloy, shot peening produced higher σ_{max} and σ_{sur}, when compared with vibratory peening. However, for cemented steel E16NCD13 vibratory peening generated higher σ_{max} and σ_{sur}, when compared to shot peening. Shot peening and vibratory peening provided similar residual stress profiles for Ti-6Al-4V titanium alloy. The evolution of residual stress profiles depends highly on the treated material. A better surface finish was provided by vibratory peening, when compared to shot peening for all studied materials. A larger surface microhardness was produced by vibratory peening for Udimet 720Li. The fatigue performances of AA7050-T7451 aluminum alloy were similar in HCF and LCF domains for shot peening and vibratory peening.

2.5.2 Effect of vibratory finishing and vibratory peening on surface integrity and fatigue life

Gane et al. [45] and Feldmann et al. [46] conducted comparative studies on the effects of vibratory finishing and vibratory peening on Ti-6Al-4V titanium alloy and the blades of blisk-rotors made of nickel based alloy, respectively. The studies focused on analysing the effects on surface roughness, compressive residual stresses and HCF performance. Gane et al. [45] carried out the vibratory finishing with abrasive triangular ceramic media of 10 mm $\times$ 10 mm and vibration amplitude of 2.5 mm. The media used for vibratory peening was 4 mm to 7 mm of hardened steel and the vibration amplitude was 4 mm. The treatment time was one hour for both processes. The processes conditions were not provided in Feldmann's work.

Surface roughness

The surface roughness measurement of Gane's study [45] on Ti-6Al-4V titanium alloy revealed that vibratory peening and vibratory finishing reduced the surface roughness R_a from a range between 0.8 and 2.9 μm to below 0.1 μm. The surface roughness was further decreased by vibratory peening. Surface roughness measurements performed by Feldmann et al. [46] on nickel based alloy showed that vibratory finishing provided a significant reduction from a value between 0.3 and 0.35 μm to 0.125 μm while vibratory peening showed a slight decrease to 0.21 μm.

Compressive residual stresses

Gane et al. [45] revealed that the σ_{max} on Ti-6Al-4V titanium alloy after vibratory peening was around -400 MPa when compared to -300 MPa after vibratory finishing. Besides, the $d_{\sigma,c}$ was larger for vibratory peening (0.175 mm), when compared to 0.1 mm for vibratory finishing. Both processes have no effect on σ_{sur} of Ti-6Al-4V titanium alloy. Feldmann et al. [46] showed that vibratory finishing produced a slight increase of compressive residual stress to -450 MPa only at the surface of blisk-rotors made of nickel based alloy, when compared to a value of -800 MPa generated by vibratory peening. The $d_{\sigma,c}$ was limited to 10 μm for vibratory finishing and was of 50 μm for vibratory peening.

Fatigue life

Gane et al. [45] performed a HCF test on a notched Ti-6Al-4V titanium alloy specimen (K_t = 1.5) with a stress ratio of R = -0.2 and a frequency of 20 Hz. They observed that vibratory peening improved fatigue life by 104%, when compared to vibratory finishing. The fatigue life scatter after vibratory finishing was larger, when compared to vibratory peening. Feldmann et al. [46] presented HCF fatigue behavior of nickel based alloy, while the fatigue test conditions were not presented. Their results revealed an increase in fatigue life of 22% for vibratory finishing and of 35% for vibratory peening.

In summary, vibratory peening produced larger $d_{\sigma,c}$ than vibratory finishing for Ti-6Al-4V titanium and nickel based alloys, higher σ_{max} for Ti-6Al-4V titanium alloy and higher σ_{sur} for nickel based alloy. Nevertheless, the surface finish induced by vibratory finishing is better than that generated by vibratory peening. Besides, vibratory peening provided better HCF life than vibratory finishing for both alloys.

2.5.3 Effect of shot peening followed by vibratory finishing (SPVF) and vibratory peening on surface integrity and fatigue life

Kumar et al. [43] compared vibratory peening to SPVF on Udimet 720Li in terms of surface roughness, residual stresses and microhardness. The shot peening was carried out using cast steel media having a diameter of 0.29 mm and a hardness of 530 HV. Vibratory finishing was subsequently carried out at a vibration amplitude of 6 mm with plastic media having a hardness of 30 HV. Vibratory peening was applied with steel media having a hardness of 510 HV and diameters of 5 - 7 mm, as well as with an amplitude of 5.5 mm. Both shot peening and vibratory peening processes were performed at same Almen intensity of 0.1 - 0.12 mmA.

The surface roughness achieved by SPVF was 0.27 μm, which was comparable to that induced by vibratory peening (0.26 μm). The σ_{sur} was larger for SPVF (-907 MPa), when compared to -640 MPa for vibratory peening alone. The σ_{max} was of -1099 MPa for SPVF and was of -874 MPa for vibratory peening. However, the depth of influence was greater for vibratory peening (200 μm) than for SPVF (160 μm). The surface micro hardness values after both processes were found to be similar and equal to 670 HV [43]. To sum up, SPVF and vibratory peening generated similar surface roughness and micro hardness at same Almen intensity. However, the induced compressive residual stress profiles were different: the σ_{sur} and the σ_{max} were larger for SPVF and the depth of influence was larger for vibratory peening. Fatigue tests are recommended to show which process is better to improve the fatigue performance of Udimet 720Li [43].

CHAPTER 3 ANALYSIS OF LITERATURE REVIEW AND OBJECTIVES

3.1 Analysis of literature review

The literature survey led to the following findings:

Vibratory peening set up

Almen intensity, processing time, vibration amplitude, frequency, media type, media mass and part position and orientation within the tub are the key parameters of vibratory peening. Almen intensity has been used in vibratory peening to compare the process effects in terms of surface roughness, residual stresses and microhardness to those resulting from shot peening. The vibration amplitude directly affects the Almen intensity. To the best of my knowledge, limited works studied the effects of vibratory peening parameters on Almen intensity. Therefore a careful study should be carried out to distinguish the effect of other vibratory peening parameters such as eccentric weights, airbags pressure, media height above the part and lubricant rate on the vibration amplitude and then define their effects on Almen intensity.

Surface integrity

The literature showed that R_a of cemented steel E16NCD13 is mainly influenced by the vibratory peening processing time. The R_a was not influenced by the increase of Almen intensity and it reached a stable value of 0.4 μm after a certain time of processing ($2T_{sat}$). Vibratory peening produced better surface finish when compared to shot peening for all the studied aerospace alloys Udimet 720Li, AA7050-T7451, Ti-6Al-4V and E16NCD13. The surface roughness evolution of those studied materials was mainly related to the process. The comparison between vibratory peening and vibratory finishing showed that the resulting surface roughness depends on the treated material. When compared to vibratory finishing, vibratory peening produced better surface finish when treating Ti-6Al-4V, but rougher surface when treating nickel based alloy. The comparison between vibratory peening and vibratory finishing showed that the resulting surface roughness depends on the treated material. The comparative study between vibratory peening and SPVF revealed that both processes generate similar surface finishes. Limited investigation of vibratory peening parameters and their effects on surface roughness was included in the literature.

Residual stresses profiles of vibratory peened cemented steel E16NCD13 showed that a higher Almen intensity, longer processing time and higher frequency yielded more compressive resid-

ual stresses profiles [5]. Vibratory peening produced larger magnitudes but shallower compressive residual stresses profiles, when compared to shot peening when treating Udimet 720Li, AA7050-T7451. For cemented steel E16NCD13, vibratory peening generated larger amplitudes and deeper compressive residual stresses than shot peening. Vibratory peening and shot peening provided similar compressive residual stresses fields for Ti-6Al-4V. Nevertheless, the literature lacks a correlation analysis of the compressive residual stresses with process parameters.

Vibratory peening had no significant effect on the surface microhardness of cemented steel E16NCD13. Higher microhardness was provided by vibratory peening when compared to shot peening, on Udimet 720Li specimens. The comparative study between vibratory peening and SPVF showed a similar microhardness when treating Udimet 720Li specimens. No comparative study that investigate the effect of vibratory peening and vibratory finishing on microhardness was available. Also, literature lacks a deep exploration of vibratory penning parameters on microhardness evolution. Therefore, a comparison of the effect of vibratory peening and shot peening on the cemented steel E16NCD13 microhardness should be carried out.

3.2 Objectives

The main objective of my project is to characterize the effects of vibratory peening on the surface roughness, residual stresses and microhardness of cemented steel E16NCD13 and compare it to shot peening. To reach this objective, the three following sub-objectives have been defined based on the points raised in the critical evaluation of literature:

• **Calibrate the process controlling parameters:** Define the relationship between the process parameters and the vibration amplitude and then investigate the effects of amplitude and other vibratory peening parameters on Almen intensity using DOE method.

• **Improve the surface integrity properties of cemented steel E16NCD13 by vibratory peening:** Target the best vibratory peening parameters combinations to provide the best compromise between better surface finish, deeper and larger residual stresses profiles and higher surface microhardness through an experimental campaign.

• **Compare the effect of vibratory peening and shot peening on surface integrity of cemented steel E16NCD13:** Carry out a comparative study on the effect of vibratory

peening and shot peening in terms of surface roughness, residual stress, microhardness of cemented steel E16NCD13.

CHAPTER 4 MATERIALS AND METHODS

4.1 Cemented steel E16NCD13

The material studied in this project is cemented steel E16NCD13, manufactured according to the ASTM 4911N standard, having the chemical composition listed in Table 4.1. The specimens provided by Safran were machined from 100 mm round bars which were milled, heat treated, and then cut to obtain the final specimens having dimensions of $60 \times 19 \times 8$ mm^3. The hardness of the cemented steel E16NCD13 is between 750 and 780 HV at the surface and between 340 and 430 HV in the bulk, with a CD around 1.1 mm (the depth where the hardness is beyond 550 HV). Its mechanical properties are listed in Table 4.2 according to ISO 683-3 standard. The average roughness R_a of the as-machined specimens was of 0.2 μm in the longitudinal direction and of 0.25 μm in the transverse direction.

4.2 Vibratory peening

4.2.1 The vibratory peening machine

Figure 4.1 shows the vibratory peening machine which was designed and manufactured by Vibra Finish (Canadian manufacturer based in Mississauga and specialized in vibratory finishing), in collaboration with Polytechnique Montréal and Safran Tech France. It was installed at CTA. The machine is equipped with a control panel, shown in Figure 4.1(b), to adjust the process parameters. The treated specimen is attached to a holder, showed in Figure 4.1(c), where Almen strips can be fixed. Almen strips types A ($76 \times 19 \times 1.3$ mm^3) and N ($76 \times 19 \times 0.8$ mm^3) were used in this work, with a hardness of 450 - 490 HV as specified in the standard SAE J442 [14]. The deflection of the strips are used to determine Almen intensity as specified in section 2.2. The holder is inserted into the tank, filled with carbon steel media diameter of 3.175 mm and hardness of 740 HV hardness, as illustrated in Figure 4.1(a) and (c). The vibration motion is provided by the eccentric weights mounted

Table 4.1 *Chemical composition of E16NCD13 alloy [47].*

Element		Fe	C	Mn	Si	Cr	Ni	Cu	Mo	P	S
Wt%	Min.	Balance	0.13	0.30	0.15	0.80	3.00	-	0.20	-	-
	Max.	Balance	0.17	0.60	0.40	1.10	3.50	0.35	0.30	0.015	0.010

Table 4.2 *Mechanical properties of normalized, annealed, case hardened and gas quenched cemented steel E16NCD13 (ISO 683-3). Young's modulus(E), Poisson's ratio (ν), density (ρ), yield stress at 0.2% ($R_{0.2}$), ultimate tensile stress (R_m), surface hardness and bulk hardness at a temperature of 23 °C are provided.*

Property	E [GPa]	ν [ ]	ρ [g.cm^{-3}]	$R_{0.2}$ [MPa]	R_m [MPa]	Surface hardness [HV]	Bulk hardness [HV]
Value	200-215	0.29	7.85	1000	1350	750-780	340-430

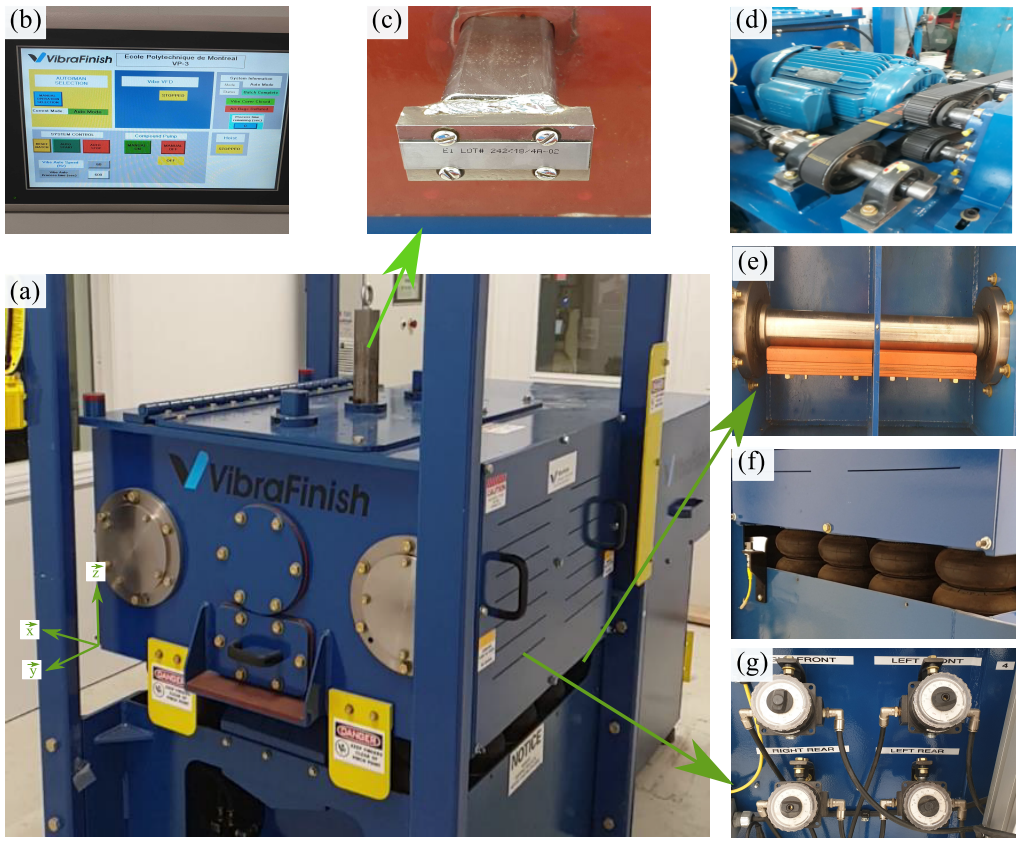

Figure 4.1 *The control parts of the vibratory peening machine. (a) The tank is full of carbon steel media of 3.175 mm and a hardness of 740 HV. (b) The control panel to control the processing time and the frequency. (c) Holder where the part is attached. The holder can be adjusted at three position (right, center, and left). (d) and (e) Eccentric weights mounted on the rotating shafts, which are driven by a motor, to provide the vibration motion. (f) and (g) Airbags whose pressure is controlled by an air pressure controller.*

on the rotating shafts, which are composed of 8 steel plates and manipulated by a motor as shown in Figures 4.1(d) and (e). The machining lubricant Castrol Syntilo 9828 is sprayed through 4 nozzles, located inside the tank, onto the media. The tank is mounted on airbags

presented in Figure 4.1(f) whose pressure is adjusted by pressure controllers (Figure 4.1(g)).

Six laser sensors were installed around the machine tub to track the movement of the tub during the process. One sensor measures the movement of the top surface, three sensors for the front surface and two on the side surface. A Labview interface was built by a technician at Polytechnique to obtain the displacements measured by the six sensors at the six surface locations of the tub. A Matlab program was developed by M.Sc. student Lucas De La Torre to simulate the tub movement to compute the amplitude and orientation of the machine in space as a function of time.

4.2.2 The vibratory peening parameters and limitation of processing domain

Definitions of the vibratory peening parameters

The vibratory peening machine is controlled mainly through the following parameters:

- X_{Mass} is defined as the media mass into the tank. The media mass ranged between 300 kg and 500 kg during the experimental campaign of Almen intensity calibration. The media mass was increased to 544 kg when defining the cemented steel E16NCD13 treatment conditions, to reach higher Almen intensities.
- X_{Ecc} is the eccentric weight per rotating shaft on the rotating shafts. It is determined by the mass of blocks fixed on the shaft. The upper limit is 8 blocks on each shaft in both sides which is equivalent to 24 kg/shaft. The lower limit is 3 kg/shaft which corresponds to 1 block by shaft.
- X_{Freq} is the rotational frequency of the rotating shafts, which is controlled by the motor speed shown in Figure 4.1(d) and is adjusted by the control panel in Figure 4.1(b). X_{Freq} can be adjusted in a range between 0 and 30 Hz.
- X_{Press} is the airbags pressure. It can be adjusted between 1 and 2.8 bars by the controllers presented in Figure 4.1(g).
- X_{Height} is the media height above the part which is defined as the height between the media surface and the treated specimen. The part holder allows a maximum X_{Height} of 32 cm. The lower limit is set as a function of the stable movement of the media.
- X_{Pos} is the part position that can be adjusted by setting the holder in one of the three holes situated on the top of the tank as shown in Figure 4.1(a).
- X_{Lub} is the lubricant flow rate in the media tank and is used to avoid media heating. It varies with the pump speed which can be adjusted between 5 and 100 rpm.

Limitation of processing parameters domain

The purpose of this section is to define the parameters domains that ensure the optimal conditions of processing. The maximum levels of X_{Ecc}, X_{Freq}, X_{Lub}, X_{Press} and X_{Mass} settled by the machine design were 24 kg/shafts, 30 Hz, 100 rpm, 2.8 bars and 544 kg, respectively.

Preliminary experiments were carried out to define the lower limit of X_{Ecc} and showed that 15 kg/shaft is the minimal modality that provides a relative media movement that ensures an energy transfer to the surface of the treated part.

X_{Ecc} was set to 24 kg/shaft when searching the lower limit of X_{Freq}. The lower frequency yielding a significant arc height equal to 0.08 mmN was 15 Hz. Therefore, the lower limit of X_{Freq} for X_{Ecc} modality of 24 kg/shaft was fixed to 15 Hz. However, for X_{Ecc} of 15 kg/shaft, the frequency of 15 Hz was insufficient to reach a significant Almen intensity. Thus, the lower modality of X_{Freq}, for X_{Ecc} of 15 kg/shaft, was increased to 23 Hz.

X_{Height} range was determined using videos recorded from the transparent window located on the side of the tank. For X_{Mass} of 500 kg, the height from the media surface to the bottom of the tank was equal to 35 cm. The recording videos showed that a stabilized movement of the media was reached when X_{Height} was equal to 10 cm. Therefore, the lower modality was set to 10 cm. To ensure that X_{Height} is the only variable when changing its modality, the part was fixed to 10 cm from the bottom of the tank when identifying the upper limit, which is equivalent to X_{Height} of 25 cm.

The depth between the media surface and the bottom of the tub for X_{Mass} of 300 kg is 20 cm. Considering the media layer of 10 cm at the top and the bottom of the tub, as for 500 kg, only one X_{Height} modality is allowed which is equal to 10 cm.

The minimal flow rate of X_{lub} that ensures the cooling of media was 20 rpm and the maximum modality that avoid lubricate leak from the tank is 50 rpm. The lower and upper modalities of X_{lub} were then set to 20 rpm and 50 rpm, respectively.

For X_{Press}, the minimal limit was fixed to 2 bars which is the lowest pressure that prevent the friction between the tank and the machine frame. Preliminary tests were performed by varying only X_{Pos}. As a result, the left and the right positions produced similar arc heights. Therefore, the modalities of X_{Pos} were setted to only center and left.

4.2.3 Methods for the control of vibratory peening parameters

The vibratory peening process was calibrated using the DOE method. In this work, by applying analysis of variance (ANOVA), the effects of X_{Ecc}, X_{Freq}, X_{Height}, X_{Pos}, X_{Lub}, X_{Press} and X_{Mass} on the Almen intensity were analysed.

DOE for vibration amplitude control

A first experimental plan was performed to define the relationship between the vibration amplitude and the vibratory peening parameters X_{Ecc}, X_{Freq}, X_{Press} and X_{Mass}. X_{Height}, X_{Pos}, X_{Lub} were not included in this first test plan since it is assumed that they don't affect the tub movement. The purpose of this experimental campaign is to define the vibration amplitude as a factor that characterizes the evolution of the parameters mentioned previously and consider it as an input covariate factor in the Almen intensity calibration plan. Table 4.3 presents the modalities of the input factors for the amplitude calibration. A split plot DOE was performed to define the individual and interactive effects of X_{Ecc}, X_{Freq}, X_{Press} and X_{Mass} on the vibration amplitude. For this purpose, a partially randomized design was applied, with 2 repetitions. Since X_{Ecc} and X_{Mass} require lengthy manual manipulations, X_{Ecc} level was changed once for each modality, X_{Mass} was changed once for each modality of X_{Ecc}. X_{Freq} and X_{Press} were fully randomized for each combination of [X_{Ecc} - X_{Mass}]. This design required $2X_{Ecc} \times 4X_{Freq} \times 3X_{Press} \times 3X_{Mass} \times 2$ repetitions = 144 tests. For each test, the machine was run for 20 seconds to get a stabilized movement of the tub without recording. Then the movement of the tub was recorded during 10 seconds using the six sensors. The signal recorded by the sensor installed at the top surface of the tub was the dominant. Therefore, each recorded signal of this sensor was treated to get the resulted amplitude of each test. The output amplitude was considered as the mean value of all recorded signals from this sensor during the test. An ANOVA was then applied to define the relationship between the vibration amplitude and the control parameters X_{Ecc}, X_{Freq},

Table 4.3 *Factors modalities of vibration amplitude calibration plan. The plan resulted in 144 tests. X_{Ecc} was changed for every modality and X_{Mass} was changed for each modality and for each X_{Mass} level. X_{Freq} and X_{Press} were fully randomized.*

Factors	**Modalities**			
X_{Ecc}(kg/shaft)	15		24	
X_{Freq}(Hz)	15	20	25	30
X_{Press}(bars)	2		2.4	2.8
X_{Mass}(kg)	300		400	500

Table 4.4 *Factors modalities of Almen intensity calibration plan. The constrained plan designed with the help of JMP software resulted in 16 tests. The plan was repeated twice with randomized execution.*

ID	X_{Ecc} (kg/shaft)	X_{Freq} (Hz)	X_{Height} (cm)	X_{Pos} (-)	X_{Lub} (rpm)	X_{Press} (bars)	X_{Mass} (kg)	Amplitude (mm)
ID01	24	15	25	Center	50	2.0	500	2.451
ID02	24	30	10	Left	50	2.8	500	3.547
ID03	15	30	10	Center	50	2.8	500	1.148
ID04	15	23	25	Left	50	2.8	500	1.294
ID05	15	30	25	Center	20	2.8	500	1.148
ID06	15	30	10	Center	20	2.8	300	1.288
ID07	15	30	10	Center	50	2.0	500	1.148
ID08	24	15	10	Left	20	2.0	500	3.678
ID09	24	15	10	Center	20	2.8	300	3.869
ID10	24	15	10	Left	50	2.8	300	4.125
ID11	24	30	25	Left	50	2.8	500	3.547
ID12	24	30	25	Left	20	2.0	300	4.011
ID13	24	30	25	Center	50	2.0	500	3.547
ID14	24	30	25	Center	50	2.0	500	3.547
ID15	15	30	10	Left	20	2.0	500	1.148
ID16	24	15	10	Center	20	2.0	500	3.678

X_{Freq} and X_{Mass}.

DOE for Almen intensity control

DOE fractional screening type was applied to obtain the relationship between Almen intensity and the eight factors: X_{Ecc}, X_{Freq}, X_{Height}, X_{Pos}, X_{Lub}, X_{Press}, X_{Mass} and the vibration amplitude as a covariate. The modalities of parameters are presented in Table 4.4. Some constraints were imposed on the plan due to the modalities reconstructions on some parameters as detailed in Section 4.2.2. The following inequations were considered when designing the plan:

$$X_{Ecc} + \frac{9}{2} X_{Freq} \geq 0, \tag{4.1}$$

$$X_{Mass} - X_{Height} \geq 0, \tag{4.2}$$

This constrained plan was designed with the help of JMP software, which resulted in 16 conditions as presented in Table 4.4, and the plan was repeated twice which resulted in 32 tests.

Figure 4.2 *Shot peening machine consists of air-compressed peening cabinet for shot peening. The media are projected from a pressurized tank into the cabinet where they shot the parts.*

4.3 Shot peening

Figure 4.2 presents the shot peening machine that was designed and manufactured by Canablast (Air powered abrasive blasting systems provider) and was installed at CTA. It hosts a 6 axis robot to monitor the position of the nozzle and a velocity sensor to measure the media velocity average. The media is projected from a pressurized tank into the cabinet where they shot the parts [48]. The used media was cast steel S110 having a nominal diameter of 0.3 mm, a hardness of 448-505 HV, a stand-off distance of 152 mm and a 10 mm nozzle diameter. The main parameters of shot peening that were controlled in this work are the air pressure and the mass flow. The air pressure ranged between 0.34 and 2 bars [0.034, 0.2 MPa] and the mass flow was varied between 2.28 and 6.8 kg/min.

4.4 Surface integrity analyses

4.4.1 Surface roughness measurements

2D roughness parameters of the peened specimens were measured with a Mitutoyo SV-C4000 series profilometer (resolution of 0.05 μm). The roughness parameters are the following: R_a represents the mean deviation of the roughness profile, R_{sk} expresses the symmetry of the peaks and valleys, R_{ku} measures the sharpness of profile peaks, RS_m indicates the mean width of the profile and R_t expresses the height between the highest peak and the lowest valley of

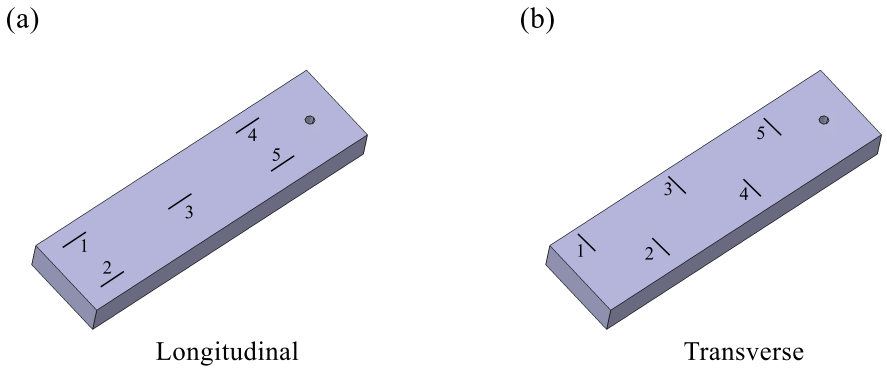

Figure 4.3 *The location of five surface roughness measurements along the (a) longitudinal direction and (b) the transverse direction.*

the roughness profile [5]. The roughness parameters were calculated in accordance with ISO 4287. Figure 4.3 shows the five selected locations for surface roughness measurements along the longitudinal and transverse directions of a specimen, respectively. It should be noted the grinding marks are along the longitudinal direction.

4.4.2 Residual stress measurements

The residual stress profiles measurements were carried out using X-ray diffraction method by the industrial partner Safran Tech France with a goniometer Stresstech Xstress 3000 G2R, 7257/7258 according to ASTM E915-16, SAE HS-784 and ISO EN15305 standards.

4.4.3 Microhardness measurements

The microhardness profiles were measured with a MVK-H0 machine (Akashi Corp) located at materials preparation and observation laboratory (LAPOM) using a force of 300 gf according to ASTM E384 standard [49]. The microhardness on each specimen was measured up to a depth of 3.02 mm with 32 indentations in total to draw the whole microhardness profile. The first measurement was taken at 0.03 mm from the surface and the first 4 indentations were taken with a pitch of $p_1 = 0.03$ mm. The pitch of the first measurements was small since the variation is higher at the surface. The following indentations were carried out with a pitch $p_2 = 0.1$ mm. Two measurement lines were then carried out with 16 measurements each. They were spaced by 0.1 mm as illustrated in Figure 4.4. The microhardness profile associated all the measurement points together.

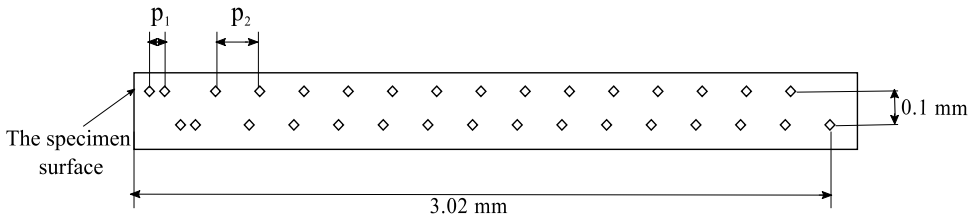

Figure 4.4 *Diagram of the positioning parameters of the microhardness measurements points. p_1 is the pitch between the first 4 indentations and p_2 is the pitch between the other 28 indentations. The spacing between two consecutive measurements is equal to 0.1 mm.*

CHAPTER 5 RESULTS AND DISCUSSIONS

5.1 Vibratory peening process control

This section provides the relationship between the machine parameters X_{Ecc}, X_{Freq}, X_{Mass} and X_{Press} with the vibration amplitude. The results of Almen intensity control plan showed in Section 4.2.3 is then presented. The last section exhibits the range of vibratory peening parameters for treating cemented steel E16NCD13.

5.1.1 Vibration amplitude control

The first DOE plan had a purpose to relate the vibration amplitude to the process parameters X_{Ecc}, X_{Mass}, X_{Freq} and X_{Press}. Figure 5.1 shows the resulting amplitude for each

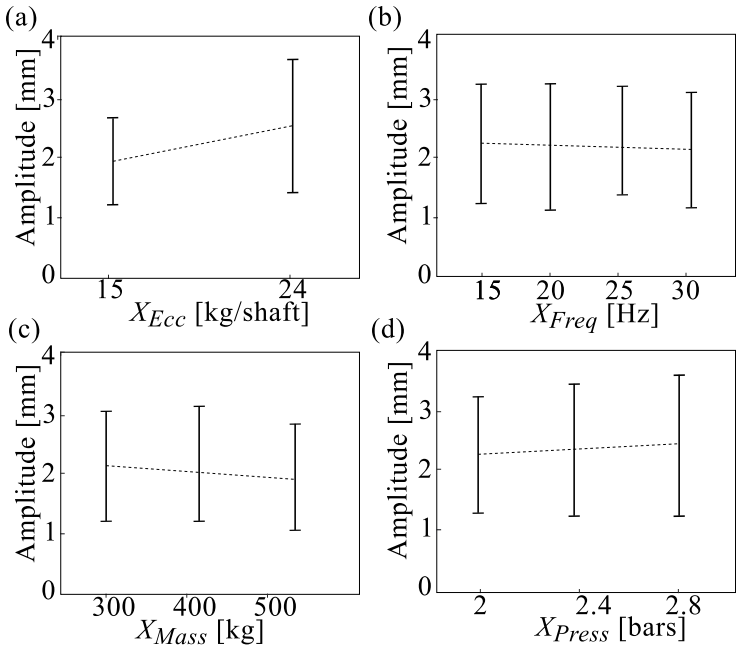

Figure 5.1 *The vibration amplitude as a function of different operation parameters.(a) X_{Ecc},(b) X_{Freq},(c) X_{Mass} and (d) X_{Press}, the intervals correspond to the vibration amplitude when fixing one parameter and varying the others. The amplitudes were obtained after data processing of laser sensors signals and it is ranged between 1.2 and 3.1 mm. X_{Ecc} graph presents the highest slope which means that it is the major factor that control the vibration amplitude variation.*

parameter modality. It reveals that the vibration amplitude varies in a range of [1.2 mm, 3.1

Table 5.1 *ANOVA analysis of vibration amplitude. The degree of freedom is the number of independent values that a statistical analysis can estimate. The sum of squares is the sum of the squares of the differences from the mean. The mean of squares is the ratio between the sum of squares and the degree of freedom. F-value is a ratio that represents how far the data are scattered from the mean. P-value below 0.01 indicates that the associated factor is statistically significant.*

Source	Degree of freedom	Sum of squares	Mean of squares	f-value	p-value
Model	10	0.6458	0.129	3.386	<0.0001
X_{Ecc}	**1**	**0.0455**	**0.0455**	**1677.5**	**<0.0001**
X_{Mass}	**1**	**0.0358**	**0.0358**	**85.515**	**0.0002**
X_{Freq}	**1**	**0.0219**	**0.0219**	**35.950**	**0.00185**
X_{Press}	1	0.0014	0.0014	1.6016	0.26
$X_{Ecc} \times X_{Mass}$	**1**	**0.0201**	**0.0201**	**27.7424**	**0.0033**
$X_{Ecc} \times X_{Freq}$	1	0.0027	0.0027	2.9818	0.1448
$X_{Ecc} \times X_{Press}$	1	0.0005	0.0005	0.2183	0.66
$X_{Mass} \times X_{Freq}$	1	0.0104	0.0104	11.6210	0.019
$X_{Mass} \times X_{Press}$	1	0.0009	0.0009	0.7032	0.44
$X_{Freq} \times X_{Press}$	1	0.0002	0.0002	2.6984	0.16
Lack of Fit	10	0.002	0.0002	1.68	0.29
Pure Error	16	0.016	0.001		
Total	36	0.6638			

mm]. The graph in Figure 5.1(a) presents the greatest slope which means that X_{Ecc} is the major parameter that influences the amplitude.

The ANOVA analysis was performed using JMP Pro software and its results are presented in Table 5.1, to develop a model that relates the vibration amplitude to X_{Ecc}, X_{Mass}, X_{Freq} and X_{Press}. The degree of freedom presents the number of independent values that a statistical analysis can estimate. The sum of squares measures the deviation of data points away from the mean value. The mean of squares is the ratio between the sum of squares and the degree of freedom. F-value is a ratio that represents how far the data are scattered from the mean and p-value is the probability of obtaining test results at least as extreme as the results observed. The ANOVA was assessed to identify the parameters and the interactions that have a significance effect on the vibration amplitude at 99% confidence interval. The p-values of amplitude model ($p < 0.01$) and lack of fit ($p > 0.01$) [50] show that the prediction model extracted from ANOVA is significant, which is appropriate. P-values which are less than 0.01 indicate that the corresponding parameters are significant on the amplitude evolution. X_{Ecc}, X_{Mass}, X_{Freq} and $X_{Ecc} \times X_{Mass}$ are the significant parameters and interactions in order of

Table 5.2 *Measured and predicted intensities resulting from the DOE plan. The constrained plan designed with the help of the JMP software resulted in 16 tests. The plan was repeated twice with randomized execution. The mean of measured Almen intensities vary between 0.0915 and 0.388 mmN. The predicted Almen intensities calculated from the model are situated in the ±5% deviation of the measured values.*

Case number	Almen intensity REP1 (mmN)	Almen intensity REP2 (mmN)	Mean	95% confidence	Predicted Almen intensity (mmN)
ID01	0.114	0.126	0.12	0.076	0.123
ID02	0.283	0.281	0.282	0.013	0.283
ID03	0.173	0.175	0.174	0.013	0.166
ID04	0.088	0.095	0.0915	0.004	0.087
ID05	0.177	0.187	0.182	0.064	0.187
ID06	0.167	0.160	0.164	0.044	0.165
ID07	0.185	0.155	0.170	0.191	0.185
ID08	0.163	0.192	0.178	0.09	0.192
ID09	0.151	0.140	0.146	0.070	0.143
ID10	0.277	0.254	0.266	0.146	0.274
ID11	0.391	0.387	0.377	0.025	0.363
ID12	0.266	0.276	0.271	0.064	0.266
ID13	0.390	0.386	0.388	0.014	0.384
ID14	0.321	0.330	0.325	0.006	0.344
ID15	0.196	0.200	0.198	0.025	0.186
ID16	0.176	0.158	0.167	0.05	0.163

quotations. Thus, after eliminating the insignificant parameters, the vibration amplitude as a function of process factors was extracted with the help of JMP Pro software and can be expressed as:

$$A = 3.3863 + 1.7228x_{Ecc} - 0.38898x_{Mass} - 0.2522x_{Freq} - 0.2204x_{Ecc}x_{Mass} \tag{5.1}$$

where A is the vibration amplitude (mm), x_{Ecc}, x_{Mass}, x_{Freq} are the coded factors of X_{Ecc}, X_{Mass}, X_{Freq}, respectively, where the upper modality of the factor is presented by +1 and the low limit is presented by -1. The values of the regression constants R^2 and adjusted R^2_{adj} are 97.8% and 95.8%, respectively, which shows a good regression of the model. Therefore, the developed vibration amplitude model is statistically fitted. The calculated amplitude was considered later as covariate. It should be noted that this model is valid in the domain studied which is for a vibration amplitude between 1.2 and 3 mm.

5.1.2 The Almen intensity control

Table 5.2 lists the resulting Almen intensities for the 16 vibratory peening conditions issued from the experimental plan specified in Table 4.4. Almen intensities varies in a range of [0.095 mmN, 0.388 mmN], which is equivalent to [0.047 mmA, 0.194 mmA], based on preliminary tests carried out on Almen strips type A that showed a coefficient $C_{A/N}$ of 0.5 between Almen intensity type A and Almen intensity type N (see Appendix A). ANOVA analysis was performed to determine the regression coefficients of the significant parameters that influence the evolution of Almen intensity using JMP software. Almen intensity as a function of processing parameters could be expressed as a second order regression equation:

$$I = b_0 + \sum b_i x_i + \sum b_{ij} x_i x_j + e_r \tag{5.2}$$

where x_i is the coded factor of X_i factor, b_i is the regression coefficient of individual factor, b_{ij} is the regression coefficient of the interaction between two factors X_i and X_j and e_r is the error term. Some iterations were performed to find a fitted model with R^2 and R^2_{adj} more than 90% and that requires the least variation of processing parameters at the same time.

The first attempt was carried out by including all the parameters X_{Ecc}, X_{Freq}, X_{Height}, X_{Pos}, X_{Lub}, X_{Press} and X_{Mass} and the interactions between them. The R^2 and R^2_{adj} of this model were equal to 99.26% and 98.56%, respectively, which indicates a good regression of the model. However, the drawback of this model is that it requires the variation of all the processing parameters. So this model was rejected. ANOVA analysis reveals that X_{Ecc} and

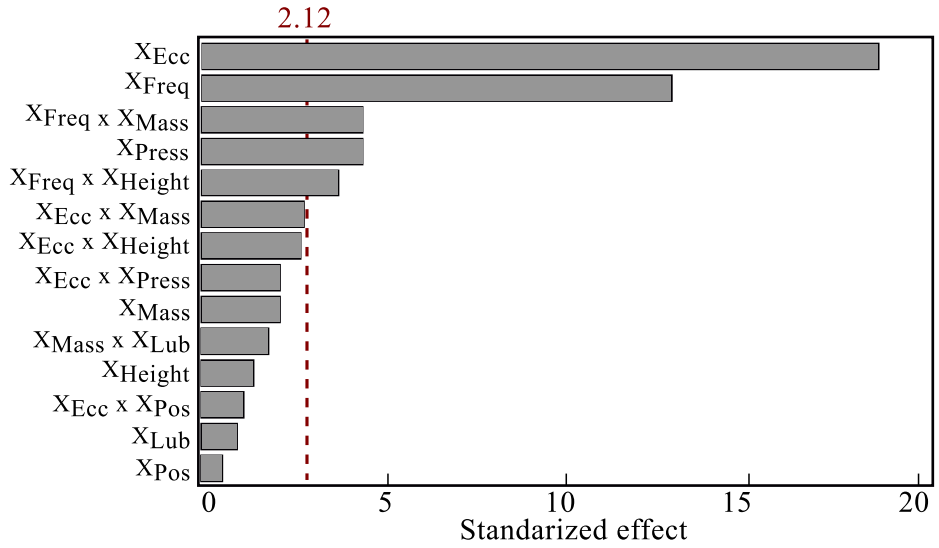

Figure 5.2 *Pareto chart of the effect of factors and their interactions for the first model of Almen intensity. The vertical red line of 2.12 corresponds to the limit of 99% of the statistical significance. All the factors or interactions having bars that extends beyond this line are considered significant.*

X_{Freq} are the major factors that control the Almen intensity. $X_{Freq} \times X_{Mass}$, X_{Press} and $X_{Freq} \times X_{Height}$ were also significant but with lower level of influence, when compared to X_{Ecc} and X_{Freq} as illustrated in Figure 5.2. The red vertical line corresponds to a limit of 99% of statistical significance. All factors and interactions having bars that extend beyond this line are considered as significant.

The second attempt was performed only with the inputs X_{Ecc} and X_{Freq}. This model possessed R^2 and R^2_{adj} of 86% and 84.51%, respectively, which are too low far from 100%, when comparing to the first model. This model was rejected also.

Therefore, the third attempt was carried out by introducing all the significant parameters obtained from the first model X_{Ecc}, X_{Freq}, X_{Press}, X_{Height} and X_{Mass}. This model revealed R^2 and R^2_{adj} of 96.65% and 93.41%, respectively, which are high enough to ensure a good model fitting. Table 5.3 shows that X_{Freq}, X_{Ecc}, their interaction $X_{Ecc} \times X_{Freq}$ and the interactions of X_{Height} with them $X_{Ecc} \times X_{Height}$ and $X_{Freq} \times X_{Height}$ are the most important factors producing p-values less than 0.01. The normality distribution of the data was analysed using the normal probability plot presented in Figure 5.3(a). It shows that all the residuals (measured value − mean value) are close to be normally distributed, which validates the choice of normal distribution for calculating confidence intervals. Figure 5.3(b) plots the predicted

values as a function of observed values of Almen intensities. The data is located in an area of ± 5% deviations which means that the proposed model fits the measured data relatively well. The regression equation extracted from this analysis, after eliminating the insignificant parameters, was:

$$I = 0.1663 + 0.0856x_{Freq} + 0.0642x_{Ecc} + 0.0216x_{Ecc}x_{Freq} + 0.0198x_{Ecc}x_{Height} + 0.0195x_{Freq}x_{Height} \quad (5.3)$$

where x_{Freq}, x_{Ecc}, x_{Height} are the coded factors of X_{Freq}, X_{Ecc} and X_{Height}, respectively. It should be noted that this model is valid only for the domain studied which is for Almen intensity ranged between 0.087 and 0.384 mmN.

Table 5.3 *ANOVA analysis of Almen intensity.*

Source	Degree of freedom	Sum of squares	Mean of squares	f-value	p-value
Model	6	0.4554	0.0759	187.2	<0.001
X_{Ecc}	**1**	**0.0151**	**0.0151**	**49.2**	**<0.001**
X_{Freq}	**1**	**0.0266**	**0.0266**	**85.5**	**<0.001**
X_{Height}	1	0.0007	0.0007	1.9	0.15
X_{Press}	1	0.0004	0.0004	1.6	0.36
X_{Mass}	1	0.0145	0.0145	27.5	0.02
$X_{Ecc} \times X_{Freq}$	**1**	**0.0085**	**0.00085**	**38.2**	**0.001**
$X_{Ecc} \times X_{Height}$	**1**	**0.0390**	**0.0390**	**66.5**	**<0.001**
$X_{Ecc} \times X_{Mass}$	1	0.0008	0.0008	3.1	0.15
$X_{Freq} \times X_{Height}$	**1**	**0.0350**	**0.0350**	**72.5**	**<0.001**
$X_{Mass} \times X_{Press}$	1	0.0009	0.0009	0.7032	0.44
$X_{Freq} \times X_{Press}$	1	0.0002	0.0002	2.6984	0.16
Lack of Fit	9	0.0029	0.0003	0.8	0.98
Pure Error	26	0.015	0.0005		
Total	41	0.4733			

5.1.3 Selection of the vibratory peening parameters range for cemented steel E16NCD13 treatment

Safran suggests treating the cemented steel E16NCD13 specimens with Almen intensities of 0.1 mmA, 0.15 mmA and 0.2 mmA. To target these Almen intensities, X_{Freq} was adjusted in a range of [20, 22.5, 25, 27.5 and 30 Hz] and X_{Height} was set to 10 and 25 cm. X_{Mass}, X_{Ecc}, X_{Press}, X_{Pos} and X_{Lub} were fixed to 500 kg, 24 kg/shaft, 2.8 bars, center and 20 rpm, respectively.

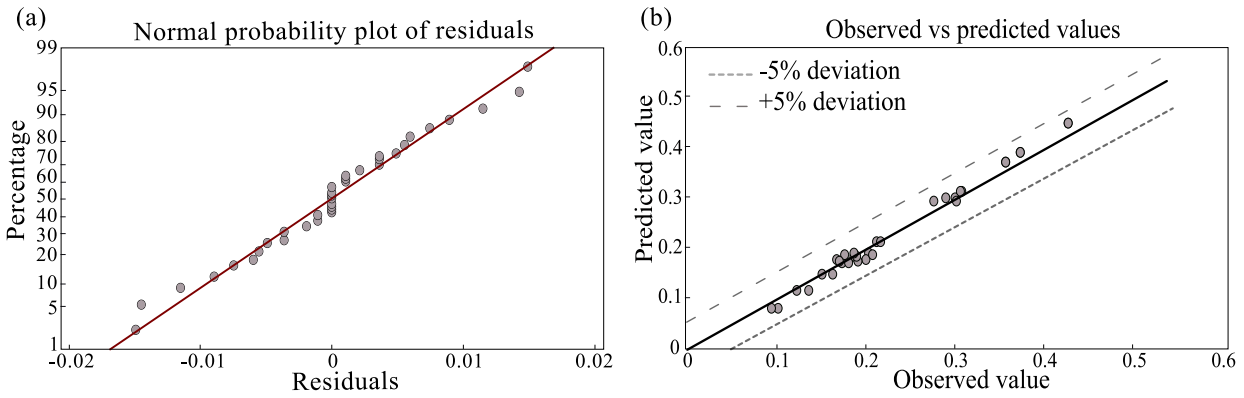

Figure 5.3 *Normal probability plots for Almen intensity. (a) The normal probability plot of residuals and (b) plot of predicted value as a function of observed value.*

Figure 5.4 presents the relationship between the experimental Almen intensity and X_{Freq} for X_{Mass} of 500 kg with the lower and the upper modalities of X_{Height}. The figure shows that, for fixed X_{Mass}, the Almen intensity increases with the increase of X_{Height}. For a X_{Mass} of 500 kg and for the two X_{Height} conditions, both curves present a drop of Almen intensity at X_{Freq} of 25 Hz for the studied frequency ranges. This phenomenon was due to the occurrence of a second mode of vibration at a frequency of 25 Hz. Under these vibratory peening conditions, the maximum resulting Almen intensity was 0.19 mmA and was lower than the target Almen intensity of 0.2 mmA. Since, both X_{Ecc} and X_{Freq} have reached their upper limits, other parameters should be adjusted to increase the resulting Almen intensity.

The DOE analysis in Section 5.1.2 shows that X_{Ecc}, X_{Freq}, X_{Height} have the most significant effects on Almen intensity. In addition, although the effect of X_{Mass} on Almen intensity was statistically insignificant, the Almen intensity calibration campaign results showed that the resulting Almen intensities obtained with $X_{Mass} = 500$ kg were higher than those with $X_{Mass} = 300$ kg. Therefore, an experimental campaign was carried out by increasing X_{Mass} from 500 kg to 544 kg to reach the target Almen intensity of 0.2 mmA. The experimental tests with $X_{Mass} = 544$ kg, X_{Freq} in a range of [17.5 Hz - 30 Hz] and X_{Height} of 17 cm and 28 cm were carried out to obtain the three targeted Almen intensities.

Figure 5.4 presents also the relationship between the Almen intensity and X_{Freq} for X_{Mass} of 544 kg. X_{Ecc}, X_{Press}, X_{Pos}, and X_{Lub} were set to 24 kg/min, 2.8 bars, center and 20 rpm, respectively. It shows that Almen intensity increased continuously with the increase of X_{Freq} and exhibits a very small drop by 0.01 mmA at $X_{Freq} = 22.5$ Hz, which is due to

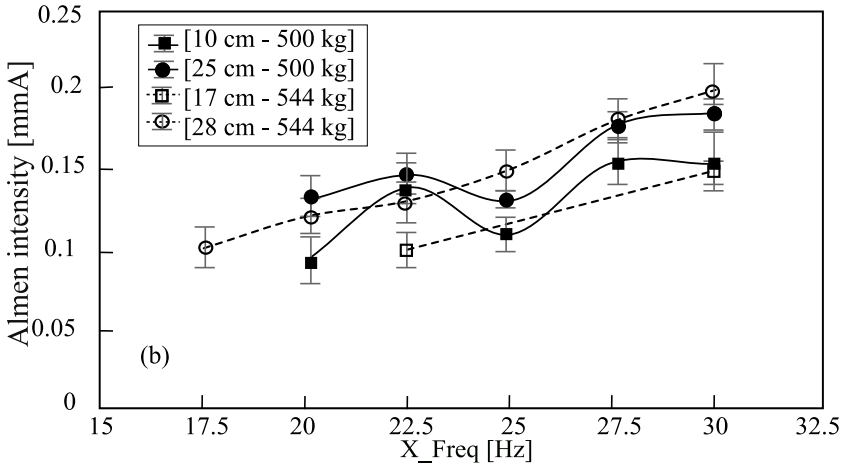

Figure 5.4 *Almen intensity as a function of X_{Freq} for different couples [X_{Height}, X_{Mass}] with 95% confidence intervals.*

the second vibration mode as explained previously for X_{Mass} of 500 kg. For X_{Height} of 28 cm, Almen intensities between 0.1 mmA and 0.2 mmA were achieved. However, for X_{Height} of 17 cm, limited Almen intensities between 0.1 mmA and 0.15 mmA were reached. Therefore, the increase of media mass to $X_{Mass} = 544$ kg could effectively increase the resulting Almen intensity to the target 0.2 mmA.

Table 5.4 lists the selected vibratory peening conditions for treating cemented steel E16NCD13 specimens. Two different vibratory peening parameters couples [X_{Height} - X_{Freq}] were applied to achieve intensities of 0.1 mmA and 0.15 mmA, respectively. The Almen intensity of 0.2 mmA was achievable only for X_{Height} of 28 cm and X_{Freq} of 30 Hz. The purpose was to study the vibratory peening effect on the surface integrity of the material treated with different process parameters while at same Almen intensities. For each of the five vibratory peening conditions, as listed in Table 5.4, three repetitions were carried out for every T_{sat} and $2T_{sat}$, which are the saturation time and double of the saturation time of Almen strip, respectively. Therefore, 5 vibratory peening conditions $\times$ 2 peening times $\times$ 3 repetitions = 30 specimens were treated by vibratory peening.

5.2 Effect of vibratory peening on surface integrity of cemented steel E16NCD13

This section presents the effect of vibratory peening on the surface proprieties of cemented steel E16NCD13 in terms of surface roughness, microhardness and compressive residual stresses, under the different treatment conditions given previously in Section 5.1.3.

Table 5.4 *Variable operation parameters, resulting Almen intensities and saturation times for the vibratory peening treatment on cemented steel E16NCD13 calibration specimens.*

Conditions	X_{Height} (cm)	X_{Freq} (Hz)	Almen intensity (mmA)	Treament time (min) $T_{sat}/2T_{sat}$
1	17	22.5	0.1	2.8/5.6
2	28	17.5	0.1	5.2/10.4
3	17	30	0.15	2.8/5.6
4	28	25	0.15	2.8/5.6
5	28	30	0.2	2/4

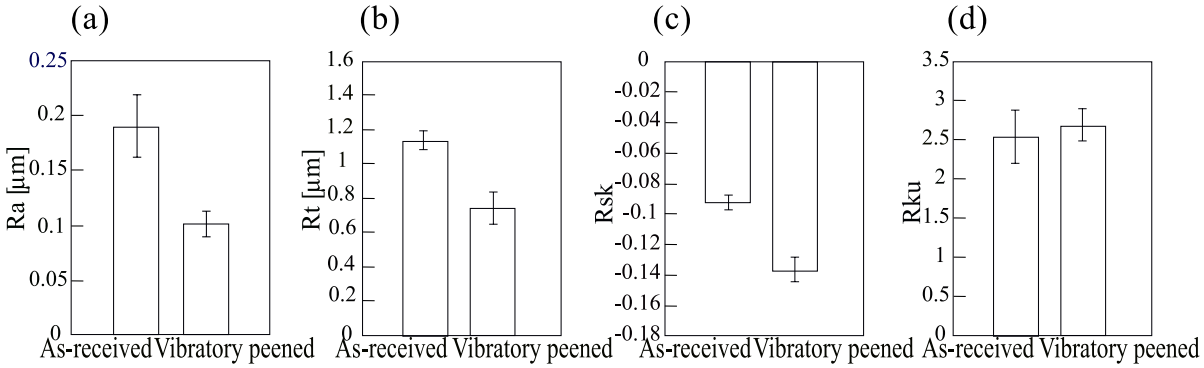

Figure 5.5 *Comparison of surface roughness parameters for as-received and vibratory peened cemented steel E16NCD13 specimens along the longitudinal direction with their* 95% *confidence intervals. (a)* R_a*, (b)* R_t*, (c)* R_{sk} *and (d)* R_{ku}*. The roughness parameters have been averaged over all specimens peened under the different conditions.*

5.2.1 Surface roughness

Figure 5.5 compares the four roughness parameters R_a, R_t, R_{sk} and R_{ku} of the as-received and the average of all the vibratory peened cemented steel E16NCD13 specimens along the longitudinal direction. Figure 5.5(a) shows that R_a decreased from 0.19 $\pm$ 0.03 μm to 0.1 $\pm$ 0.02 μm, which means that the vibratory peening process improves the surface finishing of the as-received specimen. Figure 5.5(b) shows that, when compared to the as-received specimen, vibratory peening decreased R_t from 1.15 $\pm$ 0.05 μm to 0.75 $\pm$ 0.15 μm, which means that vibratory peening reduced the total height of the roughness profile. Figure 5.5(c) reveals that R_{sk} were negative for both specimens before and after vibratory peening, which means that the valleys were larger than the peaks in both cases. In addition, the vibratory peened specimen presented more valleys, and less peaks. However, the flattening effect of vibratory peening is not pronounced since the initial peaks height was already low (-0.09 $\pm$ 0.005 μm). Figure 5.5(d) shows that vibratory peening has no significant effect on

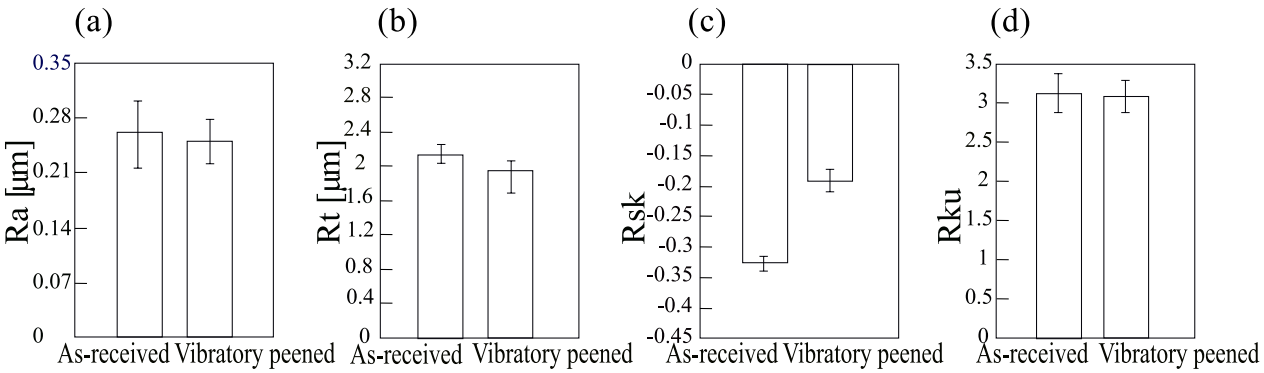

Figure 5.6 *Comparison of surface roughness parameters for as-received and vibratory peened cemented steel E16NCD13 specimens along the transverse direction with their* 95% *confidence intervals. (a)* R_a*, (b)* R_t*, (c)* R_{sk} *and (d)* R_{ku}*. The roughness parameters have been averaged over all specimens peened under the different conditions.*

R_{ku} and for both as-received and vibratory peened specimens, R_{ku} is lower than three, which indicates that the height distribution was flat and the number of high peaks and low valleys was low. In conclusion, Figure 5.5 indicates that, along the longitudinal direction, vibratory peening had a significant impact on R_a, R_t and R_{sk}, while no effect on R_{ku}.

Figure 5.6 presents the four roughness parameters R_a, R_t, R_{sk} and R_{ku} of the as-received and the average of all the vibratory peened cemented steel E16NCD13 specimens along the transverse direction. Figure 5.6(a) shows that the vibratory peening has no significant effect on R_a which can be due to the high scatter of the values. Figure 5.6(b) shows also that vibratory peening does not affect R_t along the transverse direction and that the total height of the roughness profile remains constant. Figure 5.6(c) suggests that R_{sk} was negative for both specimens before and after vibratory peening, which means that the valleys were larger than the peaks in both cases. However, R_{sk} increased from -0.33 $\pm$ 0.01 μm to -0.17 $\pm$ 0.01 μm which means that the vibratory peened specimens exhibited more peaks, when compared to as-received specimens. Figure 5.6(d) shows that vibratory peening has no significant effect on R_{ku}. For both as-received and vibratory peened specimens, R_{ku} oscillated around a value of 3 (when considering the confidence intervals), which means that the height distribution was uniform, not too high or too low. To sum up, Figure 5.6 suggests that, along the transverse direction, vibratory peening had a significant impact only on R_{sk}.

Figure 5.7 presents SEM observations of cemented steel E16NCD13 before and after vibratory peening. Figure 5.7(a) shows that the grinding marks of as received specimens are

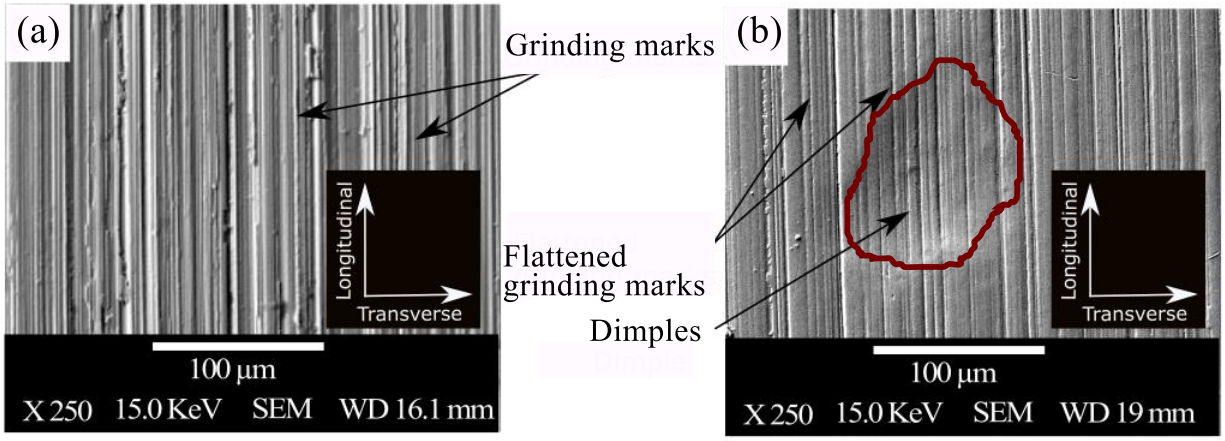

Figure 5.7 *SEM images of cemented steel E16NCD13 specimens. (a) As-received specimen showing the grinding marks direction. (b) Vibratory peened specimen at Almen intensity of 0.15 mmA for the [X_{Height} – X_{Freq}] couple of [17 cm - 30 Hz] and treatment time of 2T_{sat} showing dimples and flattened grinding marks.*

oriented along the longitudinal marks, which indicates that the surface roughness is higher along the transverse direction. Figure 5.7(b) presents a SEM image of vibratory peened specimen for the [X_{Height} – X_{Freq}] couple of [17 cm - 30 Hz]. It shows that media dimple is not perfectly spherical which provided a non uniformity of surface roughness in both directions.

Figure 5.8 shows the average roughness R_a of vibratory peened specimens at Almen intensity of 0.1 mmA for two process parameters [X_{Height} – X_{Freq}] couples of [28 cm – 17.5 Hz] and [17 cm – 22.5 Hz] along the longitudinal and the transverse directions, respectively.

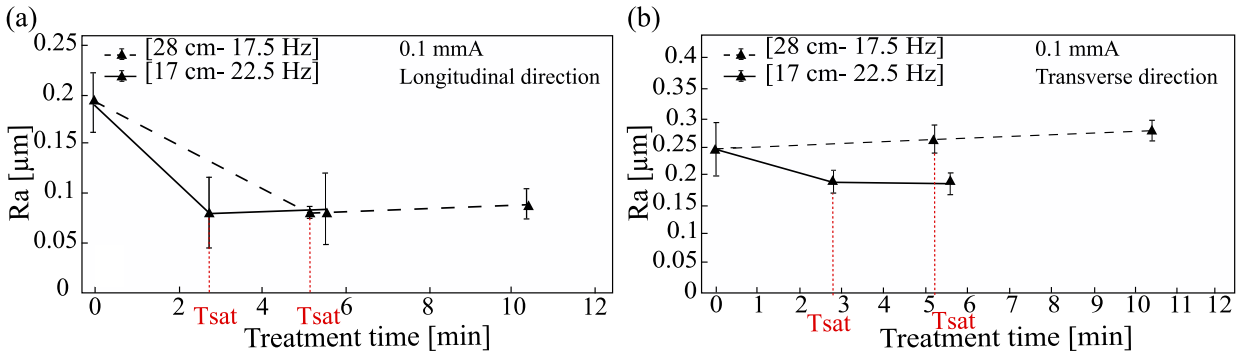

Figure 5.8 R_a *measurements for cemented steel E16NCD13 specimens with Almen intensity of 0.1 mmA (a) along the longitudinal direction and (b) along the transverse direction.*

Figure 5.8(a) reveals that R_a decreased from 0.19 ± 0.03 μm to 0.08 ± 0.03 μm along the longitudinal direction and reached this stabilized value after T_{sat} for both vibratory peening conditions. However, R_a reached this stabilized value faster for [17 cm – 22.5 Hz] couple. Figure 5.8(b) shows that for the [X_{Height} – X_{Freq}] couple of [28 cm - 17.5 Hz], R_a increased slightly from 0.25 ± 0.05 μm to 0.28 ± 0.01 μm after $2T_{sat}$ along the transverse direction. However, for the [X_{Height} – X_{Freq}] couple of [17 cm - 22.5 Hz], R_a decreased from 0.25 ± 0.05 μm to 0.19 ± 0.01 μm after T_{sat} and stabilized at this value for further treatment time.

Figure 5.9 compares the obtained R_a for specimens treated with Almen intensity of 0.15 mmA for vibratory peening parameter [X_{Height} - X_{Freq}] couples of [28 cm - 25 Hz] and [17 cm - 30 Hz] along the longitudinal direction and the transverse direction, respectively. Figure 5.9(a) shows that the effect of vibratory peening on R_a was similar for both conditions along the longitudinal direction. R_a decreased from 0.19 ± 0.03 μm to 0.1 ± 0.03 μm after T_{sat} and stabilized at this value. Figure 5.9(b) shows that along the transverse direction, for the [28 cm - 25 Hz] condition, R_a decreased slightly from 0.25 ± 0.05 μm to 0.22 ± 0.01 μm after $2T_{sat}$. However, for the [X_{Height} – X_{Freq}] couple of [17 cm - 30 Hz], it increased to 0.26 ± 0.01 μm after $2T_{sat}$.

R_a at Almen intensity of 0.2 mmA for the [X_{Height} – X_{Freq}] couple of [28 cm - 30 Hz] along the longitudinal and transverse directions, are presented in Figure 5.10. Along the longitudinal direction, R_a decreased from 0.19 ± 0.03 μm to 0.13 ± 0.01 μm after T_{sat} and stabilized at this value for an increasing treatment time, as shown in Figure 5.10(a). However, along the transverse direction, as shown in Figure 5.10(b), R_a increased slightly after T_{sat} and decreased to 0.18 μm after $2T_{sat}$. The R_a values dispersion for the as-received specimen could explain the non-monotonicity of the curve in Figure 5.10(b). Therefore, the vibratory peening has a tendency to homogenize the microgeometry of the E16NCD13 cemented steel, since the treated specimens presented lower R_a dispersion.

The following main conclusion can be drawn:

- For the as-received specimens, R_a along the longitudinal direction (0.19 ± 0.03 μm) was lower than that along the transverse direction (0.25 ± 0.05 μm), which due to the direction of the grinding marks as shown in Figure 5.7(a). Figure 5.7(b) shows the flattening grinding marks and the non-spherical shape of dimples for the [17 cm - 30 Hz] peening condition at $2T_{sat}$, which can explain the difference on the effect of vibratory peening on surface roughness along both directions.

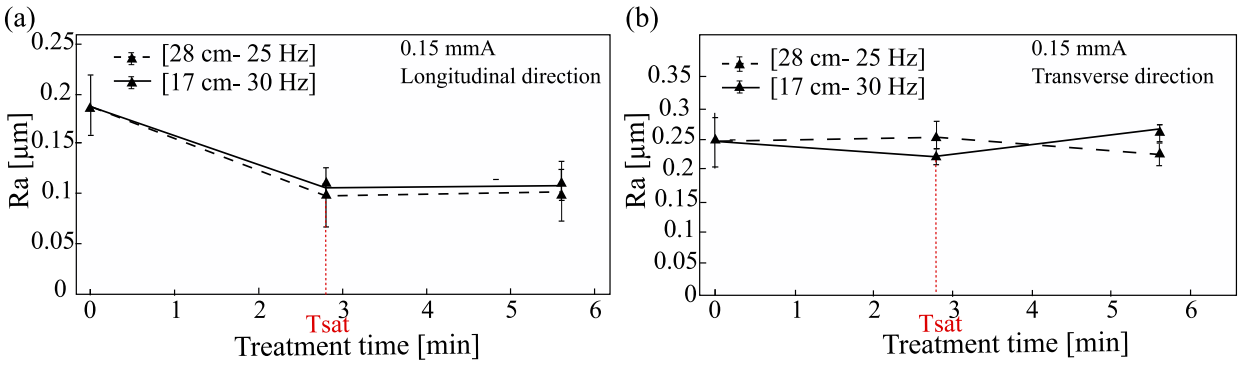

Figure 5.9 *R_a measurements for cemented steel E16NCD13 specimens with Almen intensity of 0.15 mmA (a) along the longitudinal direction and (b) along the transverse direction.*

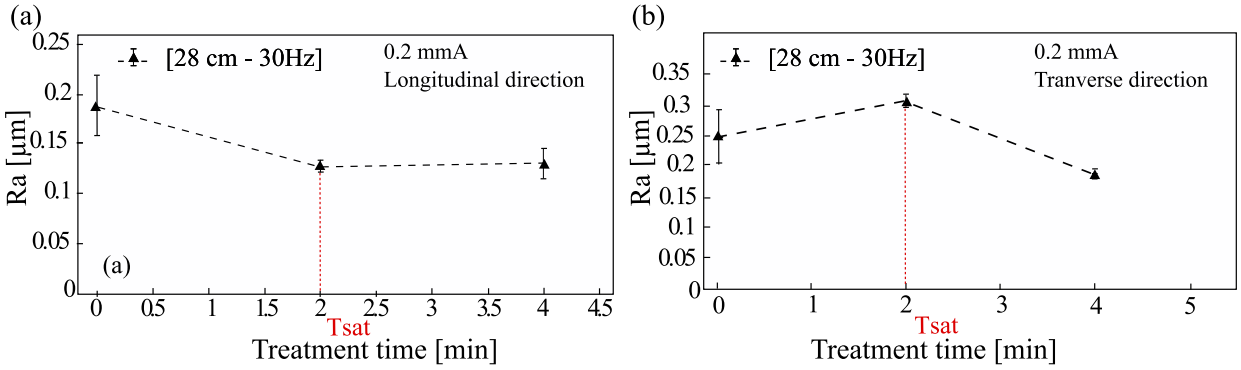

Figure 5.10 *R_a measurements for cemented steel E16NCD13 specimens with Almen intensity of 0.2 mmA (a) along the longitudinal direction and (b) along the transverse direction.*

- Along the longitudinal direction, when compared to the as-received specimens, vibratory peening decreased R_a and reached a stable value after T_{sat} for all the intensities, regardless of the process parameters. Besides, this stable R_a value increased with the increase of Almen intensity, which were 0.08, 0.1 and 0.13 μm for the Almen intensities of 0.1 mmA, 0.15 mmA, and 0.2 mmA, respectively.

- Along the transverse direction, R_a increased for a treatment time of T_{sat} and then decreased for a treatment time of $2T_{sat}$ for the case of the X_{Height} of 28 cm with Almen intensity of 0.15 mmA and 0.2 mmA. For the same Almen intensity of 0.15 mmA and X_{Height} of 17 cm, R_a decreased at T_{sat} and then increased at $2T_{sat}$. For an Almen intensity of 0.1 mmA and X_{Height} of 17 cm, R_a decreased and stabilized after T_{sat}. However, for the same Almen intensity of 0.1 mmA and X_{Height} of 28 cm, the effect of vibratory peening was not pronounced, it increased slightly by 12%. Contrary to the longitudinal direction, the effect of vibratory peening on the surface roughness along the transverse direction was highly dependent on the process parameters. This could be confirmed by the fact that the evolution of the four roughness parameters (R_a,R_t, R_{sk} and R_{ku}) were different along both directions (Figure 5.5 and 5.6). The main factors of this non-uniformity of vibratory peening effects along both directions could be due to the higher initial roughness along the transverse direction, due to the grinding marks as shown in Figure 5.7, and the non-symmetry of media dimples as shown in Figure 5.7(b).

5.2.2 Compressive residual stresses

Figure 5.11 presents the effect of vibratory peening Almen intensity on the residual stresses profile of the cemented steel E16NCD13 with Almen intensities of 0.1, 0.15, 0.2 mmA at a processing time of $2T_{sat}$ and for X_{Height} of 28 cm. The values in the curves correspond to the arithmetic mean value of the residual stresses measured in the longitudinal and the transverse directions at the same depth. The errors bars presents the uncertainty related to the X-Ray diffraction measurements, such as inadequate localization of diffraction peaks, non symmetry, a bad setting of the goniometer or incorrect adjustment of the optical system [51], which was assumed to ± 40 MPa for high strength steel.

Initial compressive residual stresses σ_c of around -150 MPa, on the as-received material, were presented and seem to be stabilized at a depth of 30 μm and increased slightly to -220 MPa at a depth of 180 μm. This layer of compressive residual stresses is due the cementation treatment. A similar σ_{sur} was observed for the intensities 0.1 and 0.15 mmA and was equal to -550 ± 40 MPa. At an intensity of 0.2 mmA, σ_{sur} of -580 ± 40 MPa was

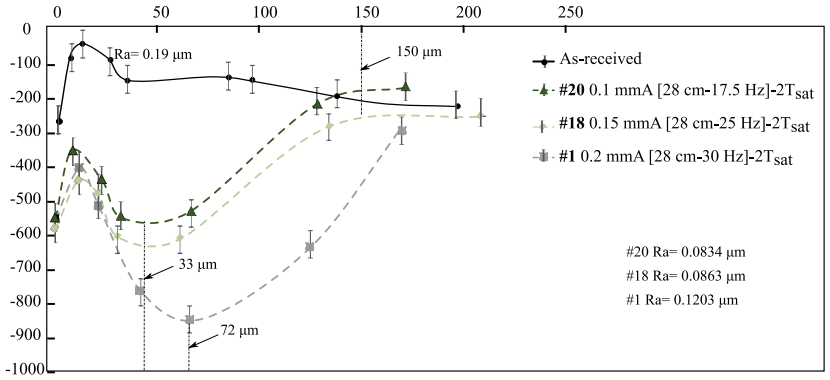

Figure 5.11 *Compressive residual stresses measurements for cemented steel E16NCD13 specimens with different Almen intensity of 0.1 mmA, 0.15 mmA and 0.2 mmA and processing time $2T_{sat}$ and X_{Height} of 28 cm.*

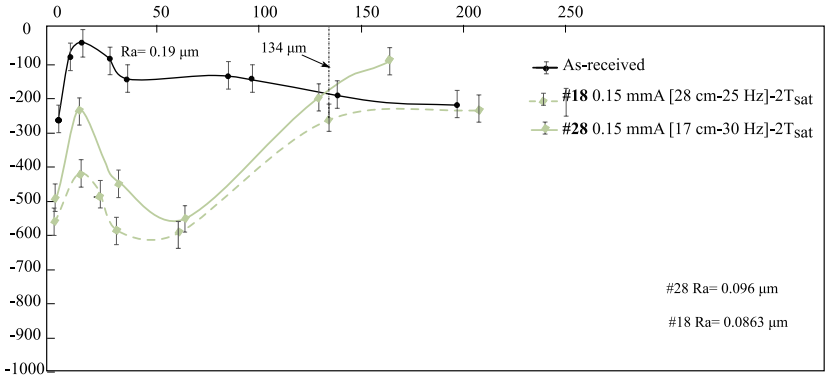

Figure 5.12 *Compressive residual stresses measurements for cemented steel E16NCD13 specimens with Almen intensity of 0.15 mmA, processing time $2T_{sat}$ and different X_{Height} 17 cm and 28 cm.*

produced. σ_{max} increased from -550 ± 40 MPa, at a depth of 33 μm, for an intensity of 0.1 mmA to -845 ± 40 MPa, at a depth of 72 μm, for an intensity of 0.2 mmA. $d_{\sigma,c}$ were similar for 0.1 and 0.15 mmA and was around 150 μm. However, $d_{\sigma,c}$ was not identified for 0.2 mmA, which requires an extension of the residual stresses measurement at this condition.

To sum up, the surface compressive residual stresses σ_{sur} increased by 5% when raising the Almen intensity from 0.1 to 0.2 mmA. The maximum compressive residual stresses σ_{max} and its depth $d_{\sigma,max}$ increased by 53% and 118%, respectively when increasing the intensity from 0.1 to 0.2 mmA. To conclude, Almen intensity has no significant influence on σ_{sur}. However the increase of vibratory peening Almen intensity produces deeper and larger compressive residual stresses. This is due to the rise of kinetic energy which produces deeper plastic deformation.

The effect of X_{Height} on the compressive residual stresses profile of vibratory peened cemented steel E16NCD13 specimens is presented in Figure 5.12. For an Almen intensity of 0.15 mmA and peening time of $2T_{sat}$, both [X_{Height} - X_{Freq}] couples of [28 cm - 25 Hz] and [17 cm - 30 Hz] were analysed. σ_{sur} and σ_{max} increased slightly with the increase of X_{Height} by 80 ± 40 MPa and 67.5 ± 40 MPa, respectively. For X_{Height} of 28 cm σ_c stabilized at $d_{\sigma,c}$ of 134 μm. However, for a X_{Height} of 17 cm the compressive residual stresses continue in decreasing. Further measurements are required to define the stabilization depth of compressive residual stresses at this condition. σ_{sur} and σ_{max} increased by 16% and 12%, respectively, when increasing X_{Height} from 17 cm to 28 cm. As a conclusion, the compressive residual stresses profiles are larger for higher X_{Height} at a constant Almen intensity. This can be explained by the fact that the deeper the specimen is inserted in the media, the more compact is the media, which can be associated to the hydrostatic pressure. An explanation for this phenomenon is yet to be provided.

The effect of vibratory peening processing time on the compressive residual stresses profile is illustrated in Figure 5.13, where the specimens were treated at T_{sat} and $2T_{sat}$ for both intensities of 0.15 and 0.2 mmA and for a constant X_{Height} of 28 cm. σ_{sur} was quasi constant for both Almen intensities and peening times and ranged from -530 ± 40 MPa to -570 ± 40 MPa. For an Almen intensity of 0.15 mmA, σ_{max} increased from -485 ± 40 MPa at $d_{\sigma,max}$ of 60 μm and peening time of T_{sat} to -620 MPa ± 40 MPa at $d_{\sigma,max}$ of 61 μm and peening time of $2T_{sat}$. The same behavior was observed at an Almen intensity of 0.2 mmA: σ_{max} increased by 85 ± 40 MPa and $d_{\sigma,max}$ raised slightly from 65 μm to 72 μm. To sum up, the processing time has an influence only on σ_{max}. It increased by 25.7% and 11.2%

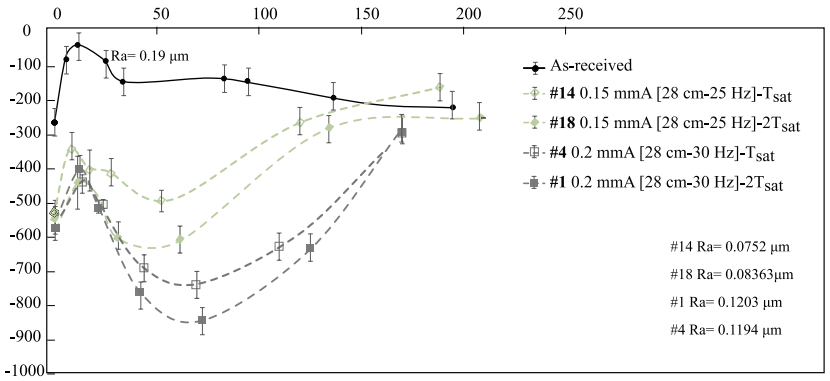

Figure 5.13 *Compressive residual stresses measurements for cemented steel E16NCD13 specimens with Almen intensities of 0.15 mmA and 0.2 mmA, X_{Height} of 28 cm and different processing time T_{sat} and $2T_{sat}$.*

respectively for 0.15 and 0.2 mmA, when the treatment time increased from T_{sat} to $2T_{sat}$. The increase of peening time yields to a larger σ_{max}. Further studies are required to identify the saturation processing time to get stabilized compressive residual stresses and identify the influence depth of vibratory peening.

5.2.3 Microhardness

Figure 5.14 presents the microhardness profiles of cemented steel E16NCD13 as-received, and vibratory peened, specimens at Almen intensities of 0.1 mmA and 0.2 mmA for a constant X_{Height} of 28 cm and X_{Freq} of 17.5 Hz and 30 Hz, respectively. The microhardness was not affected by vibratory peening for an Almen intensity of 0.1 mmA for both processing times, as shown in Figure 5.14(a). The surface microhardness increased only at an Almen intensity of 0.2 mmA. It increased from 750 ± 30 HV to 810 ± 10 HV at T_{sat} and to 850 ± 15 HV at $2T_{sat}$. However, the vibratory peening has no effect on the case depth that remains constant and equal to 1.1 ± 0.05 mm. The reason of the increase of microhardness is the plastic deformation induced by vibratory peening that increases with the increase of the processing time. The microstructural changes in the case depth caused by the transformation of the retained austenite to martensite could be also responsible for this evolution [30]. Microstructural observations are required to confirm this hypothesis.

Surface microhardness of cemented steel E16NCD13 specimens at different conditions of vibratory peening are illustrated in Figure 5.15. A significant increase of surface microhardness was observed for the couple [X_{Height} – X_{Freq}] of [28 cm - 30 Hz] at Almen intensity of

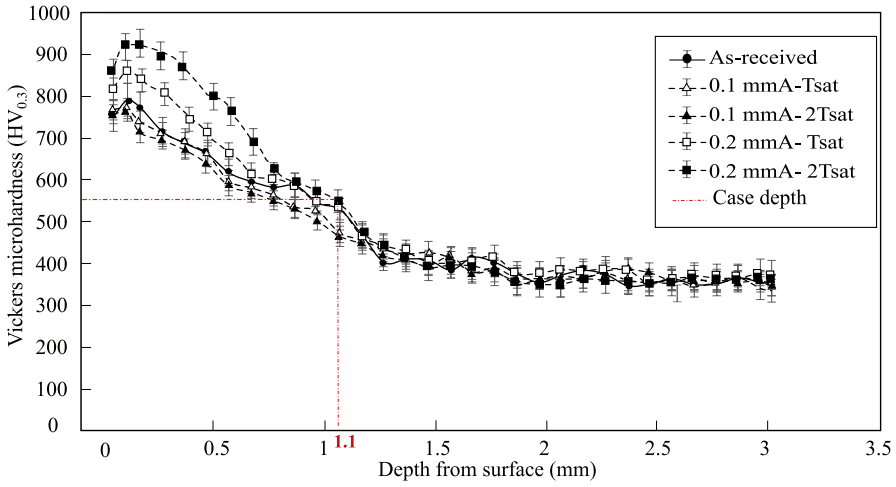

Figure 5.14 *Microhardness profiles of cemented steel E16NCD13 before and after vibratory peening for Almen intensities of 0.1 mmA and 0.2 mmA for [X_{Height} - X_{Freq}] couples of [28 cm - 17.5 Hz] and [28 cm - 30 Hz], respectively.*

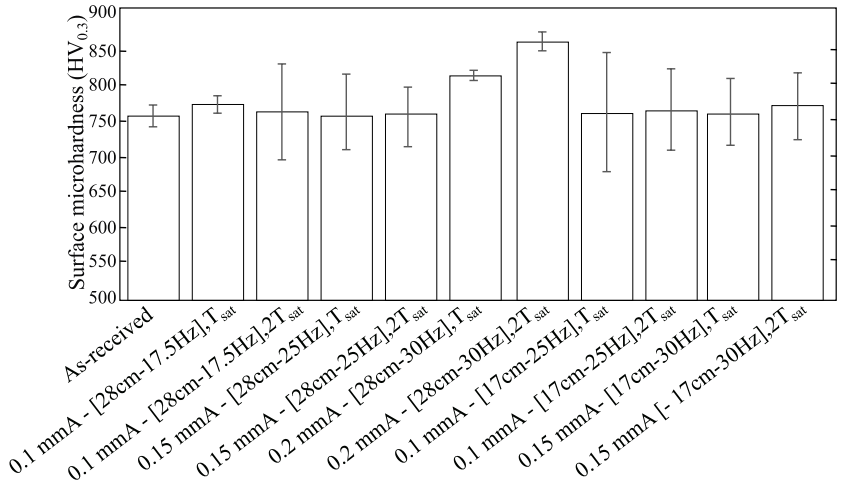

Figure 5.15 *Surface microhardness measurements with 95% confidence intervals for cemented steel E16NCD13 specimens before and after different vibratory peening conditions.*

0.2 mmA from 750 ± 30 HV to 810 ± 10 HV at T_{sat} and to 850 ± 15 HV at $2T_{sat}$. Almen intensities of 0.1 mmA and 0.15 mmA under different conditions provided similar surface microhardness.

5.3 Comparison of vibratory peening with shot peening

5.3.1 Selection of the shot peening parameters for cemented steel E16NCD13 treatment

The purpose of this section is to compare the effect of vibratory peening and shot peening on the surface integrity of cemented steel E16NCD13 specimens treated at same Almen intensities. An experimental campaign was firstly designed to find the shot peening operation parameters that produce Almen intensities of 0.1 mmA, 0.15 mmA and 0.2 mmA.

Since the air pressure and the mass flow of the media are the most important shot peening parameters influencing Almen intensity, different combinations of those two parameters were tested to reach the three target Almen intensities of 0.1 mmA, 0.15 mmA and 0.2 mmA. Table 5.5 lists the resulting Almen intensity from nine couples of [pressure - mass flow] during the campaign tests. The air pressure was adjusted in a range of [0.34 bars, 2 bars]([0.034 MPa, 0.2 MPa]) and the tested mass flows were 2.28 and 6.8 kg/min. Finally, three [pressure - mass flow] couples of [0.69 bar - 6.80 kg/min], [1 bar - 2.28 kg/min] and [1.72 bar - 2.28 kg/min] were selected to treat the E16NCD13 specimens, as listed in Table 5.6. The coverage of each shot peened specimen was evaluated according to SAE J2277 standard [19], using the VHX-7000 series digital microscope at LAPOM, with a magnification of X30 and a full ring brightness. After we define the required number of passes to reach

Table 5.5 *Shot peening conditions for the experimental campaign.*

Test number	Pressure (bar)	Mass flow (kg/min)	Almen intensity (mmA)
1	0.34	6.8	0.053
2	0.55	6.8	0.087
3	0.69	6.8	0.087
4	0.83	6.8	0.101
5	1	6.8	0.125
6	1	2.28	0.153
7	1.37	2.28	0.177
8	2	2.28	0.217
9	1.72	2.28	0.199

Table 5.6 *Parameters of the selected shot peening conditions, the resulting Almen intensities, the passes for Almen saturation on Almen strip, the passes for coverage on cemented steel E16NCD13 shot peened specimen and the treated time related to the Almen strip saturation time* T_{sat}.

Shot peening conditions	Pressure (bar)	Mass flow (kg/min)	Almen intensity (mmA)	Number of passes for saturation on Almen strips	Number of passes for 125% and 250% coverages on treated specimen	Relationship to the Almen intensity saturation time T_{sat}
1	0.69	6.8	0.1	2	10 and 20	5 and 10 T_{sat}
2	1	2.28	0.15	2.2	10 and 20	4.5 and 9 T_{sat}
3	1.72	2.28	0.2	1.6	10 and 20	6.25 and 12.5 T_{sat}

full coverage, these specimens were continuously shot peened to reach the 125% and 250% coverages. The relation between the numerical surface coverage and the number of passes is given by Equation (5.4):

$$C_n = 1 - (1 - C_1)^n \tag{5.4}$$

where C_1 is the surface coverage (decimal) after 1 pass, n is the number of passes and C_n is the coverage (decimal), after n passes.

Figure 5.16 presents the relationship between surface coverage and the shot peening passes from the experimental observation and numerical calculation by Equation (5.4). On the one side, iterative tests were performed on E16NCD13 specimens at the three Almen intensities and the coverage was visually estimated, respectively after 1 pass, 2 passes and 4 passes. The experimental coverages after four passes were 85%, 91% and 87% for 0.1 mmA, 0.15 mmA and 0.2 mmA, respectively, that were estimated visually from the optical observations according to SAE J2277 standard [19]. On the other side, the numerical calculated coverages were 92%, 90% and 86% respectively for 0.1 mmA, 0.15 mmA and 0.2 mmA. The most significant discrepancy between the coverage predicted by Equation (5.4) and that experimentally measured is of 7%, which suggests that this model could be used to predict coverage.

Using Equation (5.4), coverages after 7 and 8 passes were extrapolated as presented in Figure 5.16. Seven passes were insufficient to reach a coverage of 98% for the three intensities. Therefore, 8 passes were considered as the number of passes to get the full coverage for the three intensities according to SAE J2277 standard [19]. Note that the full coverage of specimens treated by the three intensities were validated by optical observations. According to the requirements from Safran, 125% coverage is defined as 100% to ensure the full cov-

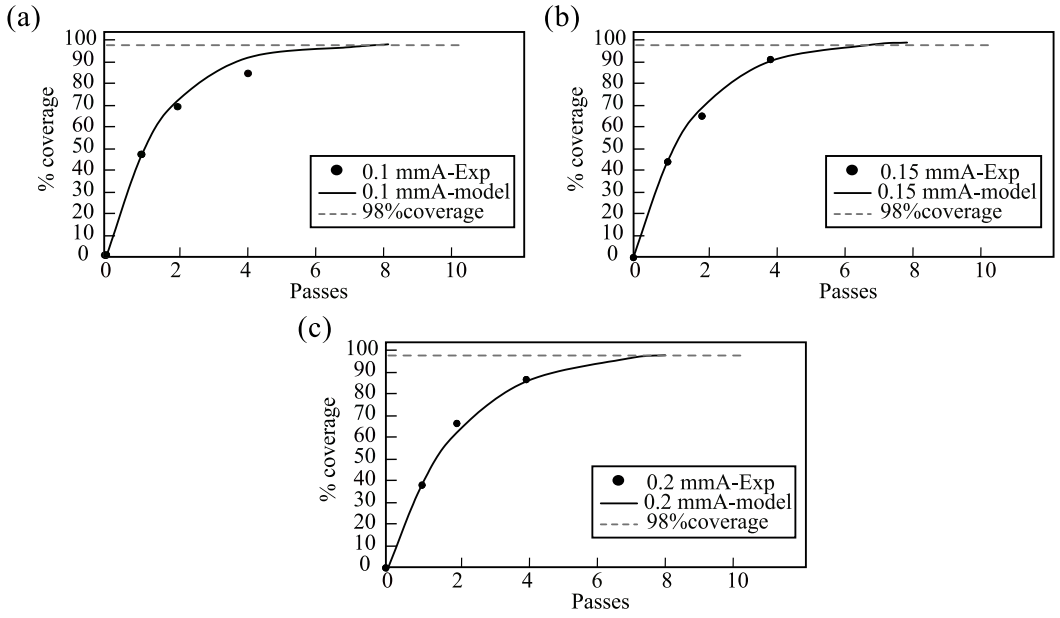

Figure 5.16 *The relationship between the shot peening surface coverage and number of passes from both experimental observation and numerical calculation from Equation (5.4) with Almen intensity of (a) 0.1 mmA, (b) 0.15 mmA and (c) 0.2 mmA.*

erage. Therefore, cemented steel E16NCD13 specimens were shot peened by 10 passes and 20 passes, in each condition, to get 125% and 250% coverages, respectively. The final shot peening operation parameters of the three selected conditions for shot peening are listed in Table 5.6.

5.3.2 Comparison with the shot peening effect on the surface integrity of cemented steel E16NCD13

Surface roughness

Table 5.7 compares the average surface roughness R_a of shot peened and vibratory peened specimens at different intensities and conditions for longitudinal and transverse directions. For the longitudinal direction, vibratory peening provided better surface finish by 60%, 58% and 35% at 0.1 mmA, 0.15 mmA and 0.2 mmA, respectively, when compared to shot peening. For the transverse direction, Almen intensity of 0.1 mmA under the condition [17 cm - 22.5 Hz], vibratory peening revealed lower surface roughness by 9.5%, when compared to shot peening. However, for the same intensity, the couple [28 cm - 45 Hz] of vibratory peening provided higher surface roughness by 33.33%. At an Almen intensity of 0.15 mmA, both conditions [17 cm - 30 Hz] and [28 cm - 25 Hz] of vibratory peening produced better

Table 5.7 *Comparison of average surface roughness R_a of E16NCD13 between vibratory peening and shot peening at different intensities.*

Almen intensity (mmA)	0.1		0.15		0.2
		Longitudinal	direction		
SP	0.2 μm		0.24 μm		0.2 μm
VP	0.08 μm		0.1 μm		0.13 μm
Difference	-60 %		-58 %		-35 %
		Transverse	direction		
SP	0.21 μm		0.33 μm		0.33 μm
VP	[17 cm - 22.5 Hz]	[28 cm - 17.5 Hz]	[17 cm - 30 Hz]	[28 cm-25 Hz]	[28 cm - 30 Hz]
	0.19 μm	0.28 μm	0.27 μm	0.22 μm	0.18 μm
Difference	-9.5 %	**+33.3** %	-18.18 %	-33.3 %	-45.45%

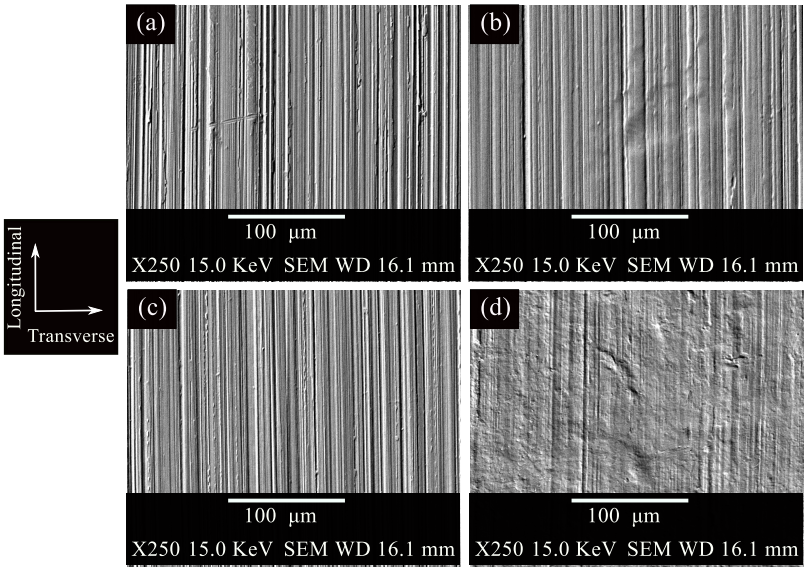

Figure 5.17 *SEM images of cemented steel E16NCD13 specimens, (a) As-received (b) Vibratory peened specimen at 0.1 mmA for the [X_{Height} – X_{Freq}] couple of [17 cm - 22.5 Hz] and treatment time of 2T_{sat} (c) Vibratory peened specimen at 0.1 mmA for the [X_{Height} – X_{Freq}] couple of [28 c m- 17.5 Hz] and treatment time of 2T_{sat} and (d) shot peened at 0.1 mmA at a coverage of 200%.*

surface finish than shot peening by 18.18 % and 33.33 %, respectively. To sum up, the vibratory peening process allows to generate better surface finish than shot peening at all the intensities. However, for an Almen intensity of 0.1 mmA for the condition [28 cm - 17.5 Hz], the vibratory peening frequency is unable to decrease the surface roughness of the treated E16NCD13 steel. In Figure 5.17(a), the as received specimen shows deep grinding marks with spacing around 3 μm. Figure 5.17(b) shows that the grinding marks spacing was enlarged and there were also flattening when peening under [17 cm - 22.5 Hz] condition. However, for the same Almen intensity and under [28 cm - 17.5 Hz] condition, the spacing between the grinding marks remains constant when comparing it with the as received condition as presented in Figure 5.17(c). This means that this frequency is insufficient to reduce the surface roughness of the cemented steel E16NCD13. Figure 5.17(d) shows that the shot peening succeed in flattened the grinding marks at 0.1 mmA. This explains the lower R_a produced by shot peening, when comparing to vibratory peening at this same intensity.

Compressive residual stresses

Figure 5.18 shows a comparison of compressive residual stresses profiles of cemented steel E16NCD13 specimens after vibratory peening and shot peening at similar intensities 0.1, 0.15 and 0.2 mmA and Table 5.8 recapitulates the residual stresses profiles important values. At all intensities, shot peening produced higher σ_{sur} than vibratory peening by 38%, 33% and 47% respectively for 0.1, 0.15 and 0.2 mmA. Also, shot peening produced higher σ_{max}, when compared to vibratory peening by 54%, 55% and 17%, respectively at 0.1, 0.15 and 0.2 mmA. However, the depth of the compressive residual stresses was larger after vibratory peening. $d_{\sigma,max}$ was higher by 50%, 110% and 132% for 0.1, 0.15, 0.2 mmA respectively. $d_{\sigma,c}$ was higher by 1.5% and 37% for 0.15 and 0.2 mmA respectively. $d_{\sigma,c}$ was not identified for shot peening at 0.1 mmA. For both processes, the depth and the magnitude of the compressive residual stresses profile increase with the increase of Almen intensity. Shot peening produced larger compressive residual stresses than vibratory peening. However, deeper profiles were provided

Table 5.8 *Comparison of average compressive residual stresses profiles of E16NCD13 after vibratory peening and shot peening at different intensities.*

Almen intensity (mmA)	0.1			0.15			0.2		
Process	SP	VP	Difference	SP	VP	Difference	SP	VP	Difference
σ_{sur} (MPa)	-760	-550	-38%	-775	-580	-33%	-810	-550	-47%
σ_{max} (MPa)	-850	-550	-54%	-950	-610	-55%	-990	-845	-17%
$d_{\sigma,max}$ (μm)	22	33	50%	29	61	110%	31	72	132%
$d_{\sigma,c}$ (μm)	-	128	-	132	134	1.5%	124	170	37%

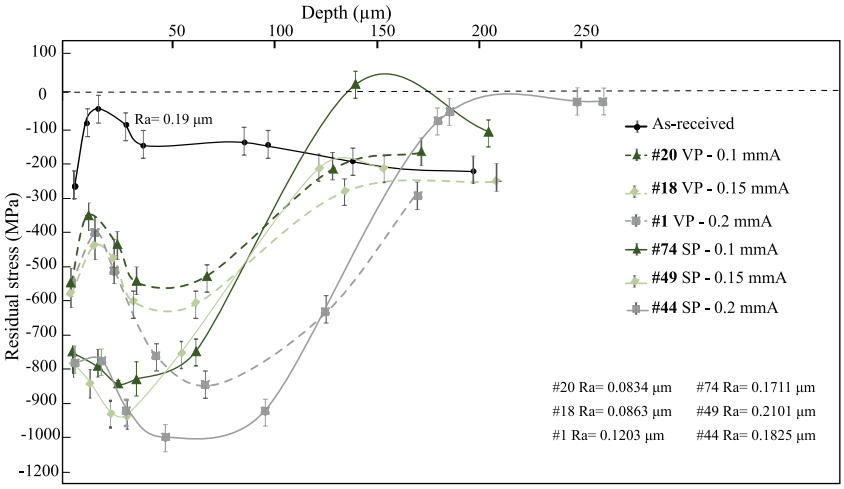

Figure 5.18 *Comparison of residual stresses profiles of cemented steel E16NCD13 specimens after vibratory peening and shot peening at Almen intensities of 0.1, 0.15 and 0.2 mmA.*

by vibratory peening. The higher $d_{\sigma,max}$ and $d_{\sigma,c}$ produced by vibratory peening could be due to the larger plastic deformation induced by the greater kinetic energy transferred to the treated piece from the media, which are larger than those used in the shot peening process.

Microhardness

Figure 5.19 compares the surface microhardness of vibratory peened and shot peened specimens at Almen intensities of 0.1 mmA and 0.2 mmA. It shows that vibratory peening increased cemented steel E16NCD13 surface microhardness only at an Almen intensity of 0.2 mmA, when compared to as-received specimens. It increased from 750 ± 30 HV to 850 ± 15 HV. However, the microhardness was almost constant after shot peening for both intensities with high dispersion at 0.1 mmA.

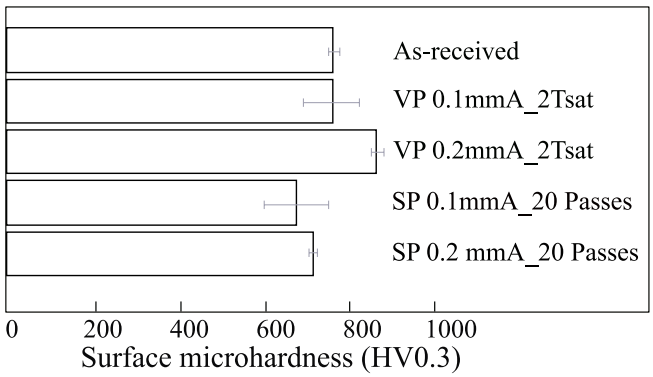

Figure 5.19 *Comparison of vibratory peened and shot peened E16NCD13 specimens surface microhardness at intensities of 0.1 mmA and 0.2 mmA.*

CHAPTER 6 CONCLUSION

6.1 Summary of works

In this work, the vibratory peening process was calibrated using the DOE technique. Therefore, the impact of vibratory peening on the surface integrity of the cemented steel E16NCD13 was investigated in terms of surface roughness, compressive residual stresses and microhardness. A comparison was finally performed with shot peening.

The calibration of the vibratory peening process allowed to survey the vibration amplitude showed that the eccentricity is the major parameter that control the tub motion. The DOE showed that the eccentricity, the frequency and the media height above the part are the major parameters that control the Almen intensity and it reveals that the vibratory peening process is able to produce intensities ranging from 0.047 mmA to 0.2 mmA.

The E16NCD13 specimens were treated by vibratory peening at the intensities 0.1, 0.15, 0.2 mmA under different machine parameters conditions. The process increased R_a, R_t and R_{sk} roughness surface parameters along the longitudinal direction (parallel to the machinig marks), while no effect was displayed on R_{ku}. Along the transverse direction (perpendicular to the machining marks), vibratory peening impacted only the R_{ku} parameter. The vibratory peening improved the surface finish of the treated E16NCD13 specimens by flattening the grinding marks. However, the non sphericity of induced dimples shape generated a difference in the surface roughness evolution along the longitudinal and transverse directions. Along the longitudinal direction, vibratory peening reduced R_a and reached a stable value after certain processing time. This stable value decreased with the decrease of Almen intensity and it ranged from 0.08 to 0.13 μm. Along the transverse direction, the R_a evolution depended mainly on machine parameters. The vibratory peening process generated a significant compressive residual stresses beneath the surface of the treated E16NCD13 specimens. The increase of the vibratory peening Almen intensity produced deeper and larger compressive residual stresses. The rise of the processing time generated higher depth of maximum compressive residual stresses. Higher media height above the part revealed larger compressive residual stresses. A slight increase of the surface microhardness was generated by vibratory peening only at an Almen intensity of 0.2 mmA. All the other peening conditions have no effect on the microhardness.

A comparative study with the shot peening process was made in terms of surface roughness, compressive residual stresses and microhardness under the intensities 0.1, 0.15 and 0.2 mmA. Along the longitudinal direction, vibratory peening provided better surface finish than shot peening for all the tested intensities and process conditions. However, along the transverse direction, certain conditions did not lead to a reduction of the surface roughness as for [28 cm - 17.5 Hz] where the frequency was too low that the process was not effective. Vibratory peening provided deeper compressive residual stresses. However, higher magnitude was generated by shot peening. Vibratory peening led to a rise of microhardness, when compared to shot peening.

To conclude, vibratory peening is able to reach intensities values between 0.047 and 0.2 mmA. This process allows to get better surface finish, except for some conditions, deeper layer of compressive residual stresses, which will delay the crack initiation and propagation, and higher surface microhardness, when compared to shot peening. This interpretation suggests that vibratory peening could provide similar fatigue behaviour as shot peening. Also, this study showed that vibratory peening can replace the shot peening and vibratory finishing processes, which can reveal a considerable enhancement in maintenance costs and an improvement of the industrial productivity. However, fatigue testing are required to validate these hypotheses.

6.2 Future research

This research project, which is a part from a big industrial project in collaboration between Polytechnique Montréal and Safran Tech France, displayed that vibratory peening is able to improve the surface integrity properties of the cemented steel E16NCD13 in terms of surface roughness, residual stresses and microhardness, which probably could lead to good fatigue life improvement. A further work is required to investigate the fatigue life at low cycle fatigue and high cycle fatigue regimes of vibratory peened E16NCD13 specimens and compare it with shot peened specimens.

The microstructure observations could be a good perspective to identify the grain sizes refinement, morphological modifications and influence depth induced by vibratory peening and investigate its relationship with the material properties changes.

REFERENCES

[1] E. Nordin and B. Alfredsson, "Experimental investigation of shot peening on case hardened SS2506 gear steel," *Experimental Techniques*, vol. 41, no. 4, pp. 433–451, 2017.

[2] J. Solis Romero, A. Anguiano García, and A. García Macedo, "Surface roughness and residual stresses on the fatigue life of shot peened components: Theoretical determination," *Ingeniería mecánica, tecnología y desarrollo*, vol. 3, no. 1, pp. 17–20, 2008.

[3] S. Gangaraj and G. Farrahi, "Side effects of shot peening on fatigue crack initiation life," *International Journal of Engineering*, vol. 24, no. 3, pp. 275–280, 2011.

[4] D. A. Davidson, "Mass finishing processes," *Metal finishing*, vol. 100, pp. 104–117, 2002.

[5] L. Canals, J. Badreddine, B. McGillivray, H. Y. Miao, and M. Levesque, "Effect of vibratory peening on the sub-surface layer of aerospace materials Ti-6Al-4V and E-16NiCrMo13," *Journal of Materials Processing Technology*, vol. 264, pp. 91–106, 2019.

[6] P. C. Williams and S. V. Marx, "Low temperature case hardening processes," Jul. 25 2000, uS Patent 6,093,303.

[7] Z. Li, A. M. Freborg, B. D. Hansen, and T. S. Srivatsan, "Modeling the effect of carburization and quenching on the development of residual stresses and bending fatigue resistance of steel gears," *Journal of materials engineering and performance*, vol. 22, no. 3, pp. 664–672, 2013.

[8] S. E. Hosseini, "Simulation of case depth of cementation steels according to fick's laws," *Journal of Iron and Steel Research, International*, vol. 19, no. 11, pp. 71–78, 2012.

[9] G. F. Vander Voort, *Atlas of time-temperature diagrams for irons and steels*. ASM international, 1991.

[10] Aubert and Duval, *Acier FADH 14NiCrMo13-4*, unknown year.

[11] T. Hong, J. Ooi, and B. Shaw, "A numerical simulation to relate the shot peening parameters to the induced residual stresses," *Engineering Failure Analysis*, vol. 15, no. 8, pp. 1097–1110, 2008.

[12] H. Miao, D. Demers, S. Larose, C. Perron, and M. Lévesque, "Experimental study of shot peening and stress peen forming," *Journal of Materials Processing Technology*, vol. 210, no. 15, pp. 2089–2102, 2010.

[13] ASTMJ443, *Procedures for Using Standard Shot Peening Test Strip, J443.* ASTM International, 2017.

[14] ——, *Test Strip, Holder, and Gage for Shot peening,J442.* ASTM International, 2017.

[15] P. Q. Trung, N. W. Khun, and D. L. Butler, "Effects of shot peening pressure, media type and double shot peening on the microstructure, mechanical and tribological properties of low-alloy steel," *Surface Topography: Metrology and Properties*, vol. 4, no. 4, p. 045001, 2016.

[16] A. Egemen, "Surface properties of AA7075 aluminium alloy shot peened under different peening parameters," *Acta Materialia Turcica*, vol. 1, no. 1, pp. 3–10, 2017.

[17] O. Unal, "Optimization of shot peening parameters by response surface methodology," *Surface and Coatings Technology*, vol. 305, pp. 99–109, 2016.

[18] H. Miao, S. Larose, C. Perron, and M. Lévesque, "An analytical approach to relate shot peening parameters to Almen intensity," *Surface and Coatings Technology*, vol. 205, no. 7, pp. 2055–2066, 2010.

[19] S. international SAE J2277, *Shot Peening Coverage Determination, J2277*, 2013.

[20] Y.-S. Nam, Y.-I. Jeong, B.-C. Shin, and J.-H. Byun, "Enhancing surface layer properties of an aircraft aluminum alloy by shot peening using response surface methodology," *Materials & Design*, vol. 83, pp. 566–576, 2015.

[21] D. C. Montgomery, *Design and analysis of experiments.* John wiley & sons, 2017.

[22] M. Bucior, L. Gałda, F. Stachowicz, and W. Zielecki, "The effect of technological parameters on intensity of shot peening process of 51CrV4 steel," *acta mechanica et automatica*, vol. 10, no. 3, 2016.

[23] E. Gadelmawla, M. M. Koura, T. M. Maksoud, I. M. Elewa, and H. Soliman, "Roughness parameters," *Journal of materials processing Technology*, vol. 123, no. 1, pp. 133–145, 2002.

[24] I. 4287, *Geometrical Product Specifications—Surface Texture: Profile Method—Terms, Definitions and Surface Texture Parameters*, 1997.

[25] J.-H. Chang, G. Liu, R. McFarland, M. Rogers, and B. Lewis, "Impact to us army fatigue qualification from shot peen process variation," 2006.

[26] C. wright, "Surface technologies shot peening applications," in *curtiss wright*, 2019.

[27] H. Ho, D. Li, E. Zhang, and P. Niu, "Shot peening effects on subsurface layer properties and fatigue performance of case-hardened 18CrNiMo7-6 steel," *Advances in Materials Science and Engineering*, vol. 2018, 2018.

[28] M. Guagliano, "Relating almen intensity to residual stresses induced by shot peening: a numerical approach," *Journal of Materials Processing Technology*, vol. 110, no. 3, pp. 277–286, 2001.

[29] D. Ciampini, M. Papini, and J. Spelt, "Characterization of vibratory finishing using the Almen system," *Wear*, vol. 264, no. 7-8, pp. 671–678, 2008.

[30] P. Renaud, "Modélisation numérique du grenaillage des pièces initialement cémentées ou carbonitrurées," Ph.D. dissertation, Ecole nationale supérieure d'arts et métiers-ENSAM, 2011.

[31] D. Bańkowski and S. Spadło, "Investigations of influence of vibration smoothing conditions of geometrical structure on machined surfaces," in *IOP Conference Series: Materials Science and Engineering*, vol. 179, no. 1. IOP Publishing, 2017, p. 012002.

[32] M. R. Baghbanan, A. Yabuki, R. S. Timsit, and J. K. Spelt, "Tribological behavior of aluminum alloys in a vibratory finishing process," *Wear*, vol. 255, no. 7-12, pp. 1369–1379, 2003.

[33] J. Domblesky, R. Evans, and V. Cariapa, "Material removal model for vibratory finishing," *International journal of production research*, vol. 42, no. 5, pp. 1029–1041, 2004.

[34] S. Naeini and J. Spelt, "Development of single-cell bulk circulation in granular media in a vibrating bed," *Powder technology*, vol. 211, no. 1, pp. 176–186, 2011.

[35] D. Ciampini, M. Papini, and J. Spelt, "Impact velocity measurement of media in a vibratory finisher," *Journal of materials processing technology*, vol. 183, no. 2-3, pp. 347–357, 2007.

[36] J.-H. Lee and K.-J. Kim, "Modeling of nonlinear complex stiffness of dual-chamber pneumatic spring for precision vibration isolations," *Journal of sound and vibration*, vol. 301, no. 3-5, pp. 909–926, 2007.

[37] K. Hashemnia, A. Mohajerani, and J. K. Spelt, "Development of a laser displacement probe to measure particle impact velocities in vibrationally fluidized granular flows," *Powder technology*, vol. 235, pp. 940–952, 2013.

[38] V. Pandiyan, S. Castagne, and S. Subbiah, "High frequency and amplitude effects in vibratory media finishing," *Procedia Manufacturing*, vol. 5, pp. 546–557, 2016.

[39] A. Sofronas and S. Taraman, "Model development and optimization of vibratory finishing process," *International journal of production research*, vol. 17, no. 1, pp. 23–31, 1979.

[40] S. Wang, R. S. Timsit, and J. K. Spelt, "Experimental investigation of vibratory finishing of aluminum," *Wear*, vol. 243, no. 1-2, pp. 147–156, 2000.

[41] J. Domblesky, V. Cariapa, and R. Evans, "Investigation of vibratory bowl finishing," *International journal of production research*, vol. 41, no. 16, pp. 3943–3953, 2003.

[42] M. D. Sangid, J. A. Stori, and P. M. Ferriera, "Process characterization of vibrostrengthening and application to fatigue enhancement of aluminum aerospace components—part i. experimental study of process parameters," *The International Journal of Advanced Manufacturing Technology*, vol. 53, no. 5, pp. 545–560, 2011.

[43] D. Kumar, S. Idapalapati, W. Wang, D. J. Child, T. Haubold, and C. C. Wong, "Microstructure-mechanical property correlation in shot peened and vibro-peened ni-based superalloy," *Journal of Materials Processing Technology*, vol. 267, pp. 215–229, 2019.

[44] H. Miao, L. Canals, B. McGillivray, and M. Lévesquea, "Comparison between vibratory peening and shot peening processes," in *Internatiol Conf. Shot Peen*, 2017, pp. 521–526.

[45] D. H. Gane, H. Rumyantsev, B. Diep, and L. Bakow, "Evaluation of vibrostrengthening for fatigue enhancement of titanium structural components on commercial aircraft," in *Ti-2003 Science and Technology, Proceedings of the 10th World Conference on Titanium, Hamburg, Germany*, 2003, pp. 1053–1058.

[46] G. G. Feldmann and T. Haubold, "Mechanical surface treatment technologies for improving hcf strength and surface roughness of blisk-rotors," in *Materials Science Forum*, vol. 768. Trans Tech Publ, 2014, pp. 510–518.

[47] SafranTech, *Document matériau -Ma-0405-12-C*, 2019.

[48] P. A. Faucheux, F. P. Gosselin, and M. Lévesque, "Simulating shot peen forming with eigenstrains," *Journal of Materials Processing Technology*, vol. 254, pp. 135–144, 2018.

[49] ASTME384, *Standard Test Method for Microindentation Hardness of Materials*. ASTM International, 2017.

[50] I. M. Fukuda, C. F. F. Pinto, C. d. S. Moreira, A. M. Saviano, and F. R. Lourenço, "Design of experiments (DOE) applied to pharmaceutical and analytical quality by design (QbD)," *Brazilian Journal of Pharmaceutical Sciences*, vol. 54, 2018.

[51] C. Meneau, P. Goudeau, P. Andreazza, C. Andreazza-Vignolle, and J. Pommier, "Caractérisation structurale et contraintes résiduelles de films d'ain par diffraction des rayons x," *Le Journal de Physique IV*, vol. 8, no. 5, pp. 5–153, 1998.

APPENDIX A CONVERSION COEFFICIENT CALCULATION BETWEEN ALMEN INTENSITY TYPE A AND ALMEN INTENSITY TYPE N

The DOE tests were all performed using Almen N strips. To get the conversion from Almen intensity type N to Almen intensity type A, some additional tests were performed using Almen A strips, as detailed in Table A.1. The conversion coefficient was calcualated as:

$$C_{A/N} = \frac{Almen\ intensity\ (mmA)}{Almen\ intensity\ (mmN)} \tag{A.1}$$

$C_{A/N}$ was equal to 0.51, 0.53, and 0.48, repsctively for AIS03, AIS06 and AIS13. $C_{A/N}$ was then considered equal to 0.5.

Table A.1 *Conversion coefficient from Almen intensity type N to Almen intensity type A. Three repetitions were performed for AIS03, AIS06 and AIS13 conditions with Almen intensity type N and type A, respectively.*

Case number	AIS03	AIS06	AIS13
Measured Almen intensity (mmN)	0.281, 0.284, 0.279	0.159, 0.167, 0.160	0.390, 0.386, 0.387
Mean Almen intensity (mmN)	0.281	0.162	0.388
Measured Almen intensity (mmA)	0.146, 0.142, 0.141	0.082, 0.090, 0.086	0.189, 0.185, 0.184
Mean Almen intensity (mmA)	0.143	0.086	0.186
$C_{A/N}$	0.51	0.53	0.48